HEALTH AND MEDICINE

The adipocyte-enriched secretory protein tetranectin exacerbates type 2 diabetes by inhibiting insulin secretion from β cells

Fen Liu[1]†, Zixin Cai[1]†, Yan Yang[1], George Plasko[2], Piao Zhao[3], Xiangyue Wu[3], Cheng Tang[3], Dandan Li[1], Ting Li[4], Shanbiao Hu[5], Lei Song[5], Shaojie Yu[5], Ran Xu[6], Hairong Luo[1], Libin Fan[1], Ersong Wang[7], Zhen Xiao[3], Yujiao Ji[1], Rong Zeng[8], Rongxia Li[8], Juli Bai[1,2], Zhiguang Zhou[1], Feng Liu[1]*, Jingjing Zhang[1]*

Pancreatic β cell failure is a hallmark of diabetes. However, the causes of β cell failure remain incomplete. Here, we report the identification of tetranectin (TN), an adipose tissue–enriched secretory molecule, as a negative regulator of insulin secretion in β cells in diabetes. TN expression is stimulated by high glucose in adipocytes via the p38 MAPK/TXNIP/thioredoxin/OCT4 signaling pathway, and elevated serum TN levels are associated with diabetes. TN treatment greatly exacerbates hyperglycemia in mice and suppresses glucose-stimulated insulin secretion in islets. Conversely, knockout of TN or neutralization of TN function notably improves insulin secretion and glucose tolerance in high-fat diet–fed mice. Mechanistically, TN binds with high selectivity to β cells and inhibits insulin secretion by blocking L-type Ca^{2+} channels. Our study uncovers an adipocyte–β cell cross-talk that contributes to β cell dysfunction in diabetes and suggests that neutralization of TN levels may provide a new treatment strategy for type 2 diabetes.

INTRODUCTION

Impaired insulin secretion due to β cell dysfunction and/or β cell loss is a major feature of diabetes. β cell dysfunction could be triggered by a variety of metabolic disorders such as glucotoxicity, lipotoxicity, oxidative responses, and inflammation (*1*). In normal physiology, insulin secretion from β cells is modulated not only by glucose but also by a variety of secretory molecules including adipokines (*2*, *3*), gut-derived hormones (*4*), myokines (*5*), and bone-derived factors (*6*). Since the discovery of leptin receptors in β cells more than 20 years ago, it has been proposed that there is an adipo-insular axis that mediates the endocrine connection between adipocytes and β cells (*7*). While dysregulated adipocyte–β cell endocrine signaling has been suggested to play a key role in impaired insulin release from β cells (*8*), the precise underlying mechanisms remain to be fully elucidated.

Pancreatic β cells synthesize and secrete insulin in a biphasic manner in response to glucose stimulation, which is pivotal for the maintenance of glucose homeostasis. After entering β cells via the high-k_m/low-affinity glucose transporter 2 (GLUT2), glucose is metabolized via glycolysis and the Krebs cycle, leading to increased cellular adenosine triphosphate (ATP)/adenosine diphosphate (ADP) ratio and subsequent closure of the ATP-sensitive potassium (K_{ATP}) channels. The closure of K_{ATP} channels results in β cell membrane depolarization and subsequent opening of the voltage-gated Ca^{2+} channel, which triggers the influx of Ca^{2+} into β cells and subsequent exocytosis of insulin-containing secretory granules (*9*). In addition to the aforementioned "triggering pathway" induced by glucose, insulin secretion from pancreatic β cells is also modulated by a number of factors such as calcium, metabolites, and secretory peptides/proteins, which mediate the cross-talk between pancreatic β cells and other tissues/cell types to maintain systemic energy homeostasis (*10*). The L-type Ca^{2+} channels (LTCCs), formed by different pore-forming α1 subunit isoforms named Cav1.1 (voltage-gated calcium 1.1), Cav1.2, Cav1.3, and Cav1.4 in association with auxiliary subunits (α2-δ, β, and γ), are essential for insulin secretion (*11*). LTCCs contain the property to conduct long-lasting and slow inactivating Ca^{2+} currents that are characterized by their high sensitivity to dihydropyridine (amlodipine, felodipine, nifedipine, isradipine), phenylalkylamine (verapamil), and benzothiazepine (diltiazem) (*12*). The two subtypes of the Cav1 channel, Cav1.2 and Cav1.3, are identified in both human and mouse islet β cells (*13*, *14*) and are responsible for Ca^{2+} influx and insulin granule exocytosis in β cells (*13*). The mRNA levels of Cav1.3 subunit, the major LTCCs subtypes in human islets (*13*), are 14.5 and 2.5 times higher than the Cav1.2 subunit mRNA level in human and mouse islet β cells, respectively (*15*, *16*), suggesting that this subtype of Cav channel plays a major role in regulating insulin secretion in human and mouse β cells.

Tetranectin (TN), which is encoded by the *Clec3b* gene, is a homotrimeric molecule of the C-type superfamily of lectins (*17*). TN was initially identified as a plasminogen-binding protein from

[1]National Clinical Research Center for Metabolic Diseases, Metabolic Syndrome Research Center, Key Laboratory of Diabetes Immunology, Ministry of Education, and Department of Metabolism and Endocrinology, The Second Xiangya Hospital of Central South University, Changsha, Hunan 410011, China. [2]Department of Pharmacology, University of Texas Health at San Antonio, San Antonio, TX 78229, USA. [3]The National and Local Joint Engineering Laboratory of Animal Peptide Drug Development, College of Life Sciences, Hunan Normal University, Changsha, China. [4]Department of Liver Organ Transplantation, The Second Xiangya Hospital of Central South University, Changsha, Hunan 410011, China. [5]Department of Urological Organ Transplantation, The Second Xiangya Hospital of Central South University, Changsha, Hunan 410011, China. [6]Department of Urology, The Second Xiangya Hospital of Central South University, Changsha, Hunan 410011, China. [7]Department of Neurosurgery, Jinshan Hospital, Fudan University, Shanghai 201508, China. [8]Key Laboratory of Systems Biology, Institute of Biochemistry and Cell Biology, Shanghai Institutes for Biological Sciences, Chinese Academy of Sciences, Shanghai 200031, China.
*Corresponding author. Email: doctorzhangjj@csu.edu.cn (J.Z.); liuf001@csu.edu.cn (F.L.)
†These authors contributed equally to this work.

human plasma (*18*), which shares an 87% amino acid sequence identity to its counterpart in mice (*19*). TN mRNA is detected in various tissues (*20*), but its protein expression is more tissue restricted (*19*–*23*). TN protein expression is positively correlated with adipogenesis in adipose tissue, and the protein has been suggested to be an adipogenic adipokine (*24*, *25*). TN interacts with a number of cellular factors including plasminogen (*26*), apolipoprotein A1 (*27*), and heparin (*28*). Several functions of TN have been reported including regulation of fibrinolysis and proteolytic processes, osteogenesis, myogenesis, Parkinson disease, and bone mineralization (*17*, *21*, *29*, *30*). There are some studies showing that TN is inversely associated with coronary artery disease (*31*, *32*) and heart failure (*33*). However, the role of TN in diabetes remains obscure. One study found that plasma TN levels were elevated in poorly controlled type 1 diabetes (T1D) children compared with age-matched healthy subjects (*34*). However, a proteomic study found that serum TN concentration was decreased in the type 2 diabetes (T2D) individuals (*31*).

In this study, we identify TN as a fat-enriched secreted molecule that contributes to β cell dysfunction in diabetes. Serum levels of TN are greatly elevated in diabetic humans and mice compared to their respective controls. Suppressing or increasing TN expression improves or attenuates, respectively, glucose tolerance in mice. TN binds with high selectivity to human and mouse islet β cells, and TN treatment attenuates glucose-stimulated insulin secretion (GSIS) in β cells by inhibiting the LTCCs. Our results uncover a likely adipocyte–β cell endocrine signaling pathway that inhibits β cell function in diabetes, suggesting that suppressing TN expression and/or function may be a valuable approach for improving β cell function in diabetes.

RESULTS

The serum levels of TN are up-regulated in diabetic humans and mice

To elucidate the mechanisms underlying the metabolic syndrome (MS) and T2D in humans, we performed deep proteomic profiling of human sera from normal control ($n = 10$), obesity group ($n = 7$), and MS patient group with varied MS symptoms such as central obesity, hyperglycemia, hyperlipemia, and/or hypertension ($n = 5$) (table S1). Using fold change ≥ 2.0 and $P < 0.05$ as the cutoff criteria, we detected 59 molecules from a total of 704 proteins whose expression levels were significantly different between healthy human subjects and patients with obesity and/or MS (Fig. 1A and fig. S1A). Several of these genes were greatly reduced in patients with MS, including proteins involved in the complement and coagulation cascade, immunity, and calcium binding (Fig. 1A). On the other

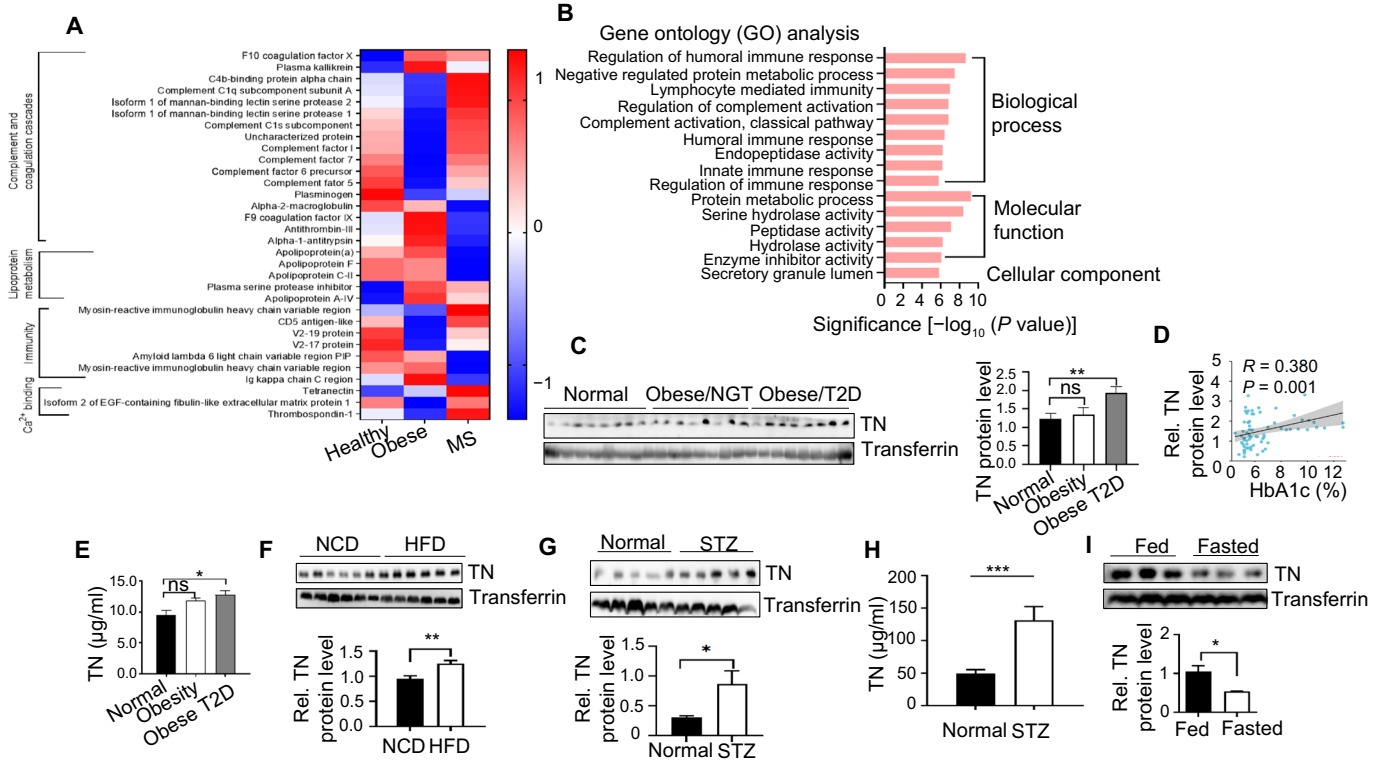

Fig. 1. The serum levels of TN are up-regulated in diabetic humans and mice. (**A**) Heatmap depicting the serum level differences of selected genes in normal, obese, and MS human subjects. (**B**) GO analysis of the cellular component, molecular function, and biological process in DEGs. Fold enrichment threshold was set at >2 and Bonferroni-corrected for $P < 0.05$. (**C**) Western blot for serum TN levels from normal controls, obese NGT, and obese T2D male patients. Transferrin was used as an internal control ($n = 24$ per group). The Western blot data were semiquantified with an ImageJ program (**$P < 0.01$). (**D**) Association between serum TN levels and HbA1c status in the serum of normal, obese NGT, and obese T2D male patients ($n = 72$). (**E**) ELISA for plasma TN concentrations in normal, obese NGT, and obese T2D male patients. (**F**) Serum TN levels in HFD-fed male mice ($n = 6$ per group) were detected by Western blot. (**G**) Serum TN levels in STZ-treated male mice ($n = 6$ per group) were detected by Western blot. (**H**) ELISA for plasma TN concentrations in STZ-treated male mice ($n = 8$ to 13 per group). (**I**) Serum TN levels in fasted male mice ($n = 6$ per group) were detected by Western blot. Data are expressed as means ± SEM; ns, not significant. *$P < 0.05$, **$P < 0.01$, and ***$P < 0.001$.

hand, the expression levels of several proteins involved in lipoprotein metabolism [plasminogen activator inhibitor 3 (gene name: *Serpina5*) and apolipoprotein A-IV (gene name: *Apoa4*)] and calcium binding (TN; gene name *Clec3b*) were notably increased in patients with MS compared to healthy controls (Fig. 1A). Gene ontology (GO) enrichment analysis revealed that pathways related to peptidase activity, immune response, protein metabolism, and complement activation were markedly enriched within the differentially expressed genes (DEGs) (Fig. 1B). To further confirm the MS-associated increase in serum TN levels, we analyzed a new group of age- and sex-matched human patients (tables S2 and S3). We found that the serum levels of TN were significantly higher in both male (Fig. 1C) and female (fig. S1B) patients with both obesity and T2D but not obese patients with normal glucose tolerance (NGT) (Fig. 1C and fig. S1B) compared to lean controls. Spearman's rank correlation and linear regression analysis showed that TN serum levels were positively correlated with hemoglobin A1C (HbA1c) (Fig. 1D and fig. S1C) but not age or BMI (table S4). By an enzyme-linked immunosorbent assay (ELISA), we found that serum TN concentrations were around 10 μg/ml in healthy humans, which is significantly higher in obese human patients with T2D (Fig. 1E). The serum and adipose tissue TN expression levels, which are compatible between male and female mice (fig. S1, D and E), were markedly increased in two diabetic mouse models, the high-fat diet (HFD)–fed (Fig. 1F) and streptozotocin (STZ)–induced (Fig. 1, G and H) diabetes mice. Serum TN levels were significantly reduced in overnight-fasted mice compared to ad libitum–fed mice (Fig. 1I).

Identification of TN as a fat-enriched secreted molecule in mice

Quantitative polymerase chain reaction (qPCR) analysis revealed that TN mRNA expression was highly enriched in human (Fig. 2A) and mouse (Fig. 2B) adipose tissues. Consistent with these results, high levels of TN protein were detected in human subcutaneous white adipose tissue (sWAT) and epididymal WAT (eWAT), as well as mature adipocytes isolated from these tissues (Fig. 2C and fig. S1F). TN is also highly expressed in mouse brown adipose tissue (BAT), sWAT, eWAT, and, to a much lesser extent, the muscle, heart, and kidney (Fig. 2D). No signal was detected in tissues from TN knockout ($TN^{-/-}$) mice (Fig. 2D), demonstrating the specificity of the antibody. TN protein expression was found by immunohistochemical staining in mouse and human islets (*35*, *36*). However, we detected no TN mRNA (fig. S1G) and protein (fig. S1H) in islets of wild-type (WT), TN heterozygote ($TN^{+/-}$), and $TN^{-/-}$ mice. Consistent with a very recent finding that TN expression is increased during adipogenesis (*25*), we found that both TN mRNA (Fig. 2, E and F) and protein expression or secretion (Fig. 2, G and H) were markedly induced during 3T3-L1 and brown fat cell (BFC) differentiation, which correlated with the protein or mRNA expression of adiponectin (Fig. 2G and fig. S1I) and uncoupling protein 1 (UCP1) (Fig. 2H and fig. S1J), the differentiation marker for 3T3-L1 adipocytes and BFCs, respectively. The expression and secretion of TN were greatly stimulated by glucose in differentiated adipocytes via a concentration-dependent mechanism, and the expression could be induced by glucose as low as 5.5 mM (Fig. 2I). Consistent with these results, STZ- and HFD-induced hyperglycemia significantly increased TN

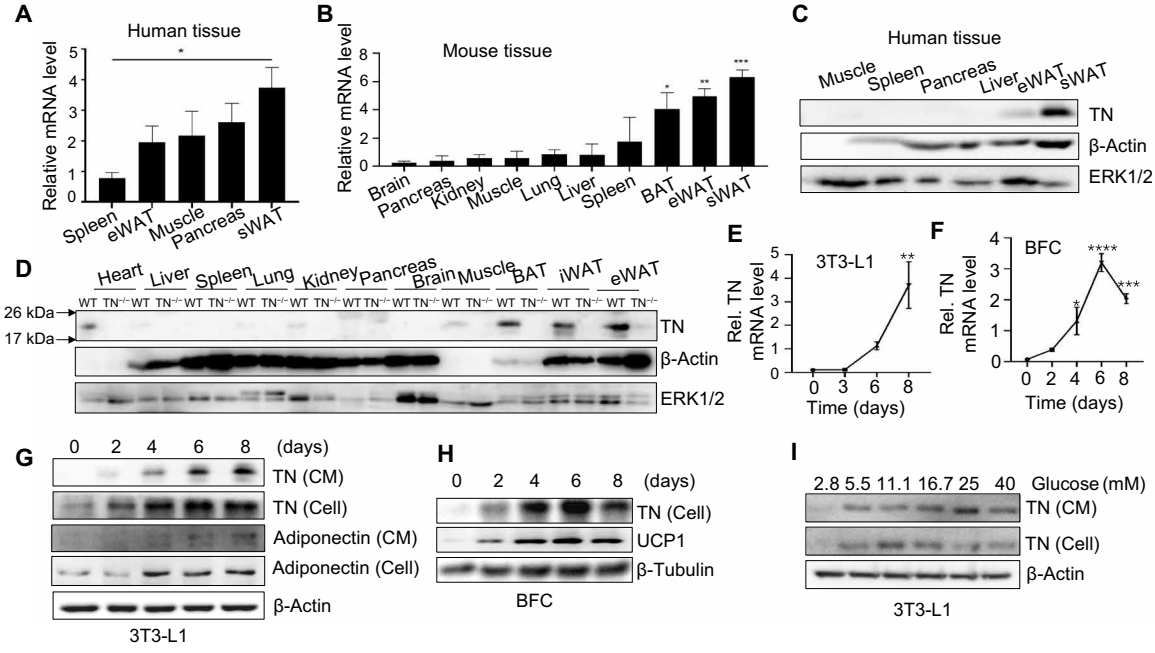

Fig. 2. Identification of TN as a fat-enriched secreted molecule in mice. (**A** to **D**) TN mRNA (A and B) or protein (C and D) expression in various human (A and C) or male mouse (B and D) metabolic tissues were determined by qPCR or Western blot, respectively. TN mRNA expression during 3T3-L1 adipocyte (**E**) and BFC (**F**) differentiation. *$P < 0.05$, **$P < 0.01$, ***$P < 0.001$, and ****$P < 0.0001$ compared with day 0 during adipocyte differentiation. Values are expressed as means ± SEM. (**G** and **H**) Western blot showing the TN protein levels in culture medium (CM) or cell lysates (Cell) during 3T3-L1 adipocyte (G) and BFC (H) differentiation. Adiponectin or UCP1 is shown as a differentiation marker of 3T3-L1 adipocytes or BFC, respectively. (**I**) TN protein levels in CM and cell lysates of mature 3T3-L1 adipocytes treated with a range of glucose concentrations for 48 hours. Data in (A) to (I) are representative of three independent experiments with similar results. Data are expressed as means ± SEM; *$P < 0.05$, **$P < 0.01$, ***$P < 0.001$, and ****$P < 0.0001$.

expression in sWAT and eWAT (fig. S1, K, L, N, and O) but had little effect on TN expression in BAT (fig. S1, M and P), heart, muscle, and kidney (fig. S1, Q to V). These findings reveal that glucose-induced TN expression occurs mainly in WAT.

To elucidate the mechanism by which high glucose stimulates TN expression, we assessed the gene expression profile in human adipocytes treated with low or high levels of glucose by transcriptome sequencing analysis. Analysis of the DEGs revealed 125 genes whose expression was significantly different between these two groups (fold change ≥ 2.0, $P < 0.05$), where 102 of them were up-regulated and 23 down-regulated in the high-glucose group compared to the low-glucose group (the top 20 significantly DEGs were shown in fig. S2A). GO and pathway analysis using $P < 0.05$ as the cutoff criteria revealed that the most significantly enriched GO terms are those involved in cartilage development, motile cilium, and growth factor activity (fig. S2B). Functional annotations of these DEGs revealed that the top enriched pathways were linked to signal transduction (fig. S2C). By reverse transcription PCR (RT-PCR), we examined the mRNA expression of 10 up-regulated DEGs and found that the gene encoding the thioredoxin-interacting protein (TXNIP) is significantly up-regulated in response to high-glucose treatment in human adipocytes differentiated from stromal vascular fraction (SVF), 3T3-L1 adipocytes, and BFCs (Fig. 3, A and B, and fig. S2D). Suppressing *Txnip* by small interfering RNA (siRNA) significantly reduced glucose-stimulated expression of *Clec3b* (Fig. 3, C and D), the gene coding TN in human adipocytes. On the basis of the finding that p38 mitogen-activated protein kinase (MAPK) mediates high glucose–stimulated TXNIP expression (*37*), we asked whether inhibition of p38 MAPK has an effect on TN expression. We found that inhibition of p38 MAPK by SB203580 significantly suppressed glucose-stimulated TN mRNA (fig. S2E) or protein (fig. S2F) expression in 3T3-L1 adipocytes. In addition, suppressing p38 by siRNA inhibited high glucose–induced TN expression (Fig. 3, E and F). Given that TXNIP promotes oxidative stress by inhibiting the activity (*38*) and protein expression (*39*) of thioredoxin, we examined the effect of thioredoxin on glucose-induced TN expression. We found that the glucose-induced TN mRNA (Fig. 3G) and protein (Fig. 3H) expression was markedly decreased by treating 3T3-L1 cells with thioredoxin. Glucose regulates several transcription factors including ChREBP, PPARγ, OCT4, and Nanog (*40*–*42*). OCT4 is also regulated by thioredoxin (*42*–*44*). Thus, we asked whether OCT4 is involved in high glucose–stimulated TN expression. We found that knockdown *Oct4* by siRNA significantly reduced high glucose–induced TN mRNA and protein expression (Fig. 3, I and J). These results suggest that high glucose may promote TN expression via the p38 MAPK/TXNIP/thioredoxin/OCT4 pathway.

TN binds with high selectivity to human and mouse islet β cells

To identify the target tissues of TN action, we examined the binding of TN fused to the secreted alkaline phosphatase (SEAP-TN) to various

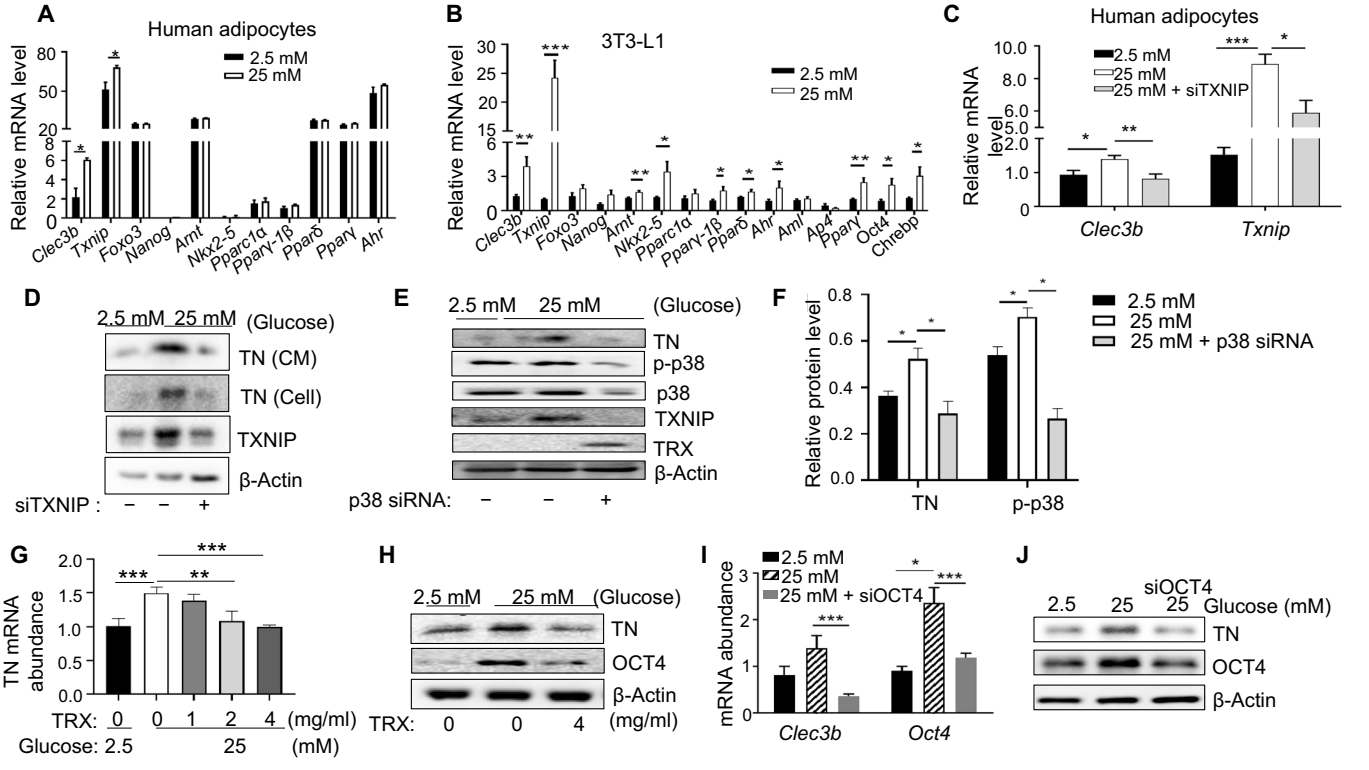

Fig. 3. TXNIP/thioredoxin mediates high glucose–induced TN expression in adipocytes. The glucose-induced gene expression was determined by qPCR in SVF-differentiated human adipocytes (**A**) and 3T3-L1 adipocytes (**B**). mRNA (**C**) and protein (**D**) levels of TN and TXNIP in scrambled or *Txnip*-siRNA–suppressed SVF-differentiated human adipocytes treated with glucose for 24 hours. (**E** and **F**) Protein levels of TN and TXNIP in scrambled or p38-siRNA–suppressed 3T3-L1 adipocytes treated with low (2.5 mM) or high (25 mM) glucose for 24 hours. The mRNA (**G**) and protein (**H**) levels of TN in 3T3-L1 adipocytes treated with low or high glucose for 24 hours in the presence of absence of different concentrations of thioredoxin were determined by qPCR and Western blot, respectively. Expression of gene (**I**) and protein (**J**) of *Clec3b* in OCT4-suppressed 3T3-L1 cells. Data in (A) to (J) are representative of three independent experiments with similar results. Data are expressed as means ± SEM; $^{*}P < 0.05$, $^{**}P < 0.01$, and $^{***}P < 0.001$.

mouse tissues. We found that SEAP-TN bound with high selectivity to mouse pancreas and islets and, to a lesser extent, the liver and muscle (Fig. 4A and fig. S3A). The binding of SEAP-TN to the pancreas tissue section was competitively blocked by preincubation of His-TN (20 mg/ml) (Fig. 4B), confirming the specificity of this binding. A strong SEAP-TN binding signal was also detected in the human pancreas and islet tissue sections (Fig. 4C), suggesting a potential role of TN in regulating human pancreatic islet function. TN could also bind to pancreas from T2D patients, and the degree of binding is greater than that of the healthy subjects (Fig. 4C).

TN impairs glucose tolerance in mice

To explore the physiological role of TN in vivo, we analyzed the metabolic phenotype of male $TN^{-/-}$ mice and WT control mice fed a normal chow diet (NCD) or an HFD. TN was undetectable in the serum of $TN^{-/-}$ mice (fig. S3B), and there were no significant differences in body weight, food intake, fat mass, lean mass, and various tissue weight between $TN^{-/-}$ and WT mice fed either an NCD or an HFD (fig. S3, C to J). Glucose tolerance was also similar between $TN^{-/-}$ mice and WT littermates fed an NCD (fig. S3K). However, under HFD feeding conditions, $TN^{-/-}$ male and female mice displayed a significantly improved glucose but not insulin tolerance compared to WT mice (Fig. 5, A and B, and fig. S3, L and M). Consistent with these findings, both basal and glucose-stimulated insulin secretion (Fig. 5C and fig. S3N) as well as random serum insulin level (fig. S3O) were increased in HFD-fed $TN^{-/-}$ male and female mice compared to WT control mice. To determine the potential role of TN in β cell function, we examined blood glucose levels and glucose tolerance over time in a low-dose STZ-induced diabetic mouse model. Low-dose STZ injection induced a severe diabetic phenotype in WT control mice that persisted throughout the entire 60-day study, with an average blood glucose level exceeding 400 mg/dl during ad libitum feeding (Fig. 5D). Under similar conditions, the $TN^{-/-}$ mice displayed increased resistance to STZ-induced diabetic symptoms, better glucose tolerance, and improved glucose control and survival (Fig. 5, D to F). TN has a half-life of approximately 8 hours, and intraperitoneal injection of His-tagged recombinant TN (body weight of 1 mg/kg) led to an approximately six times increase in serum TN levels (fig. S3P). TN injection exacerbated glucose intolerance in both NCD- and HFD-fed C57BL/6J mice (Fig. 5, G and H) and reduced GSIS during the intraperitoneal glucose tolerance test (IPGTT) (Fig. 5I). Consistent with the finding that knockout of TN had no significant effect on insulin tolerance, TN intraperitoneal injection in vivo had little effect on insulin sensitivity in both NCD- and HFD-fed C57BL/6J male mice (fig. S3, Q and R). We further tested the effects of long-term TN administration (1 mg/kg; every day for 2 weeks) in 4-month-old NCD-fed male C57BL/6J mice. There were no significant differences in body weight and food intake between TN- and vehicle-treated mice (fig. S3, S and T). However, long-term TN administration significantly attenuated the scavenging activity of glucose in HFD-fed mice (Fig. 5J). To further confirm the role of TN in glucose metabolism, we administrated a TN neutralization antibody or control immunoglobulin G (IgG) into HFD-fed mice. Administration of the anti-TN antibody but not IgG significantly reduced blood glucose levels and increase random insulin levels in both HFD-fed mice and db/db mice, which is a model with persistent β cell failure (Fig. 6, A to D), suggesting that reducing TN levels is sufficient to improve HFD-induced glucose intolerance in mice.

Liraglutide alleviates diabetes by improving β cell function (*45*). To determine whether the beneficial effect of liraglutide is mediated by suppressing TN action, we treated WT and $TN^{-/-}$ mice with liraglutide. Liraglutide treatment improved IPGTT in both $TN^{-/-}$ and WT mice (fig. S4A). In addition, liraglutide treatment had no effect on the expression of TN in adipocytes (fig. S4B). These results suggest that liraglutide treatment and TN suppression improve β cell function via distinct mechanisms. To determine whether the combination of anti-TN neutralizing antibody and liraglutide has an additive effect on hyperglycemia in mice, we treated HFD-fed C57/BL6 mice daily with the TN neutralizing antibody (2 mg/kg per day, subcutaneous injection) or control IgG together with liraglutide (100 μg/kg per day, subcutaneous injection) or saline for 60 days. IPGTT and HbA1c levels were comparable among different treatment groups before the TN antibody and liraglutide treatment (fig. S4, C to E). In agreement with the finding of others (*46*, *47*), liraglutide treatment alone significantly improved insulin resistance and body

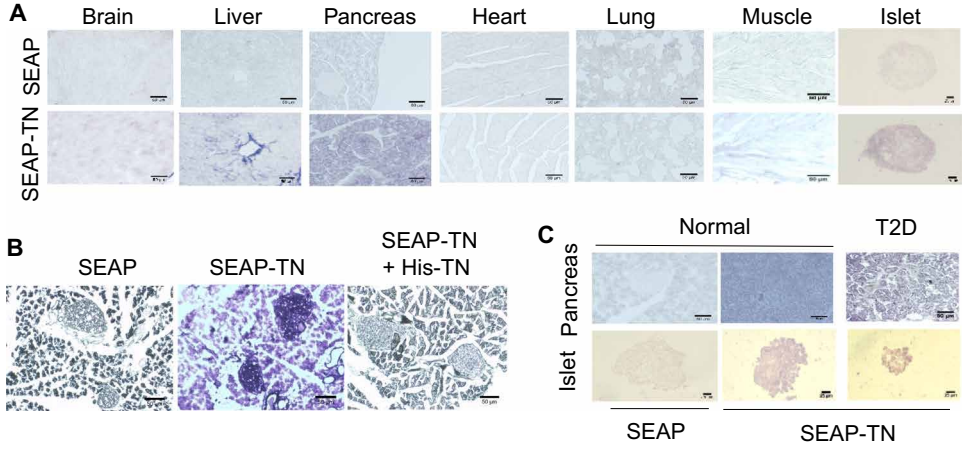

Fig. 4. TN binds with high selectivity to human and mouse islet β cells. (**A**) Binding of SEAP or SEAP-TN to various frozen mouse tissue and islet sections ($n = 6$ per condition). (**B**) Binding of SEAP-TN to mouse pancreas sections in the presence or absence of excess recombinant His-TN ($n = 6$ per condition). (**C**) Binding of SEAP-TN to frozen human pancreas and human islets. Data in (A) to (C) are representative of three independent experiments with similar results ($n = 6$ per condition). Four to eight sections of each pancreas were covered. Scale bars, 50 μm (scale bars of islets, 25 μm).

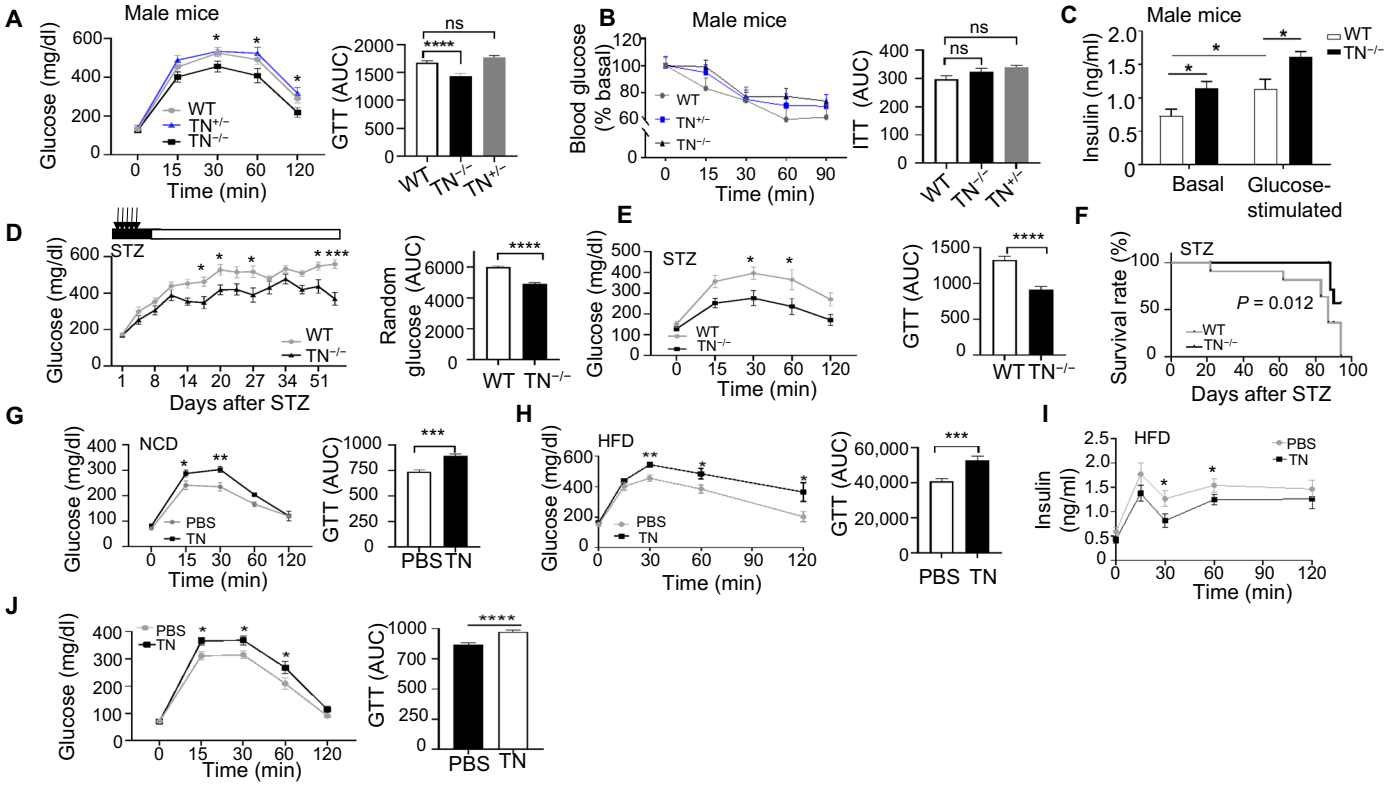

Fig. 5. TN impairs glucose tolerance in mice. IPGTT (**A**) and IPITT (**B**) in male WT, TN heterozygous mice ($TN^{+/-}$), and TN knockout mice ($TN^{-/-}$) fed an HFD for 16 weeks ($n = 9$ to 12 mice per genotype). Area under the curve (AUC) data are shown. (**C**) Insulin secretion has been measured either in the absence of glucose (baseline) or for 10 min after the glucose stimulation in male WT and $TN^{-/-}$ mice fed an HFD for 16 weeks. Results are presented as the difference in concentration between glucose stimulation and baseline ($n = 6$ mice per genotype). (**D**) WT or $TN^{-/-}$ male mice were treated with STZ daily from day 1 at 45 mg/kg for 5 days. Random-fed blood glucose levels were monitored every other day for 60 days after the first STZ injection ($n = 12$ mice per genotype). Black arrows indicate days of STZ injection (first 5 days). (**E**) IPGTT experiment was performed on the STZ-treated male mice on day 8 after STZ injection ($n = 7$ per genotype). (**F**) Survival curve of the STZ-treated male WT and $TN^{-/-}$ mice ($n = 11$ to 12 mice per genotype). Male C57BL/6J mice fed an NCD (**G**) or HFD (**H**) were intraperitoneally injected with phosphate-buffered saline (PBS) or affinity-purified His-TN (1 mg/kg). IPGTT experiments were performed in mice on the same day after TN injection ($n = 6$ to 12 per treatment group). (**I**) Insulin levels during an IPGTT of male HFD mice ($n = 11$ to 12 mice per genotype). (**J**) IPGTT experiments were performed in the male mice at the 11th day after TN injection ($n = 8$ per treatment group). Values are expressed as means ± SEM; ns, not significant. $^{*}P < 0.05$, $^{**}P < 0.01$, $^{***}P < 0.001$, and $^{****}P < 0.0001$.

weight (Fig. 6, E and F). In addition, both liraglutide and the TN neutralizing antibody significantly improved IPGTT and HbA1c levels (Fig. 6, G and H). The glucose-lowering effect was further enhanced when the HFD-fed mice were cotreated with both the anti-TN neutralizing antibody and liraglutide (Fig. 6, G and H), revealing an additive effect of the combined treatment on improving hyperglycemia.

TN suppresses glucose-stimulated insulin release in human and mouse β cells

In hyperglycemic clamp studies, we found that $TN^{-/-}$ mice exhibited a significantly higher glucose infusion rate (GIR) compared to WT littermates when fed an NCD (Fig. 7A). The insulin secretion rate of the $TN^{-/-}$ mice was also significantly higher than that of the WT littermates during the hyperglycemic clamp studies (Fig. 7B). To determine the mechanism by which TN deficiency improves β cell function, we first examined β cell morphology in $TN^{-/-}$ and WT control mice. There was no significant difference in islet morphology (fig. S4F) as well as β and α cell mass (fig. S4, G and H) between the HFD-fed $TN^{-/-}$ mice and WT control mice. Knockout of TN in mice also had no significant effect on islet proliferation, dedifferentiation, and apoptosis, as demonstrated by similar ratio of insulin-Ki67 double-positive nuclei (fig. S4I), similar numbers of insulin and Ngn3 (fig. S4J), and similar insulin-TUNEL (terminal deoxynucleotidyl transferase–mediated deoxyuridine triphosphate nick end labeling) double-positive nuclei (fig. S4K), respectively, between the HFD-fed $TN^{-/-}$ mice and WT control mice. There was also no significant difference in the differentiation between $TN^{-/-}$ mice and WT control mice (fig. S4L). Consistent with these findings, TN had no significant effect on the expression of genes involved in differentiation, proliferation, apoptosis, endoplasmic reticulum stress, inflammation, and autophagy (fig. S4, M to P). These findings suggest that TN may inhibit insulin secretion by targeting a step in the insulin secretory pathway rather than by affecting overall β cell physiology. TN treatment reduced GSIS by 30 to 50% in human (Fig. 7C) and mouse (Fig. 7D) islets. TN treatment also impaired *KCl*-induced, a depolarizing agent, insulin secretion in mouse islets (Fig. 7E). Total islet insulin content is similar between the control and TN-treated human or mouse islets (fig. S5, A and B). In vitro perfusion experiment showed that TN suppressed insulin secretion in human and mouse islets perfused with either high glucose, which closes the K_{ATP} channels, or high K^+ concentration, which induces membrane depolarization (Fig. 7, F and G). These results suggested that TN

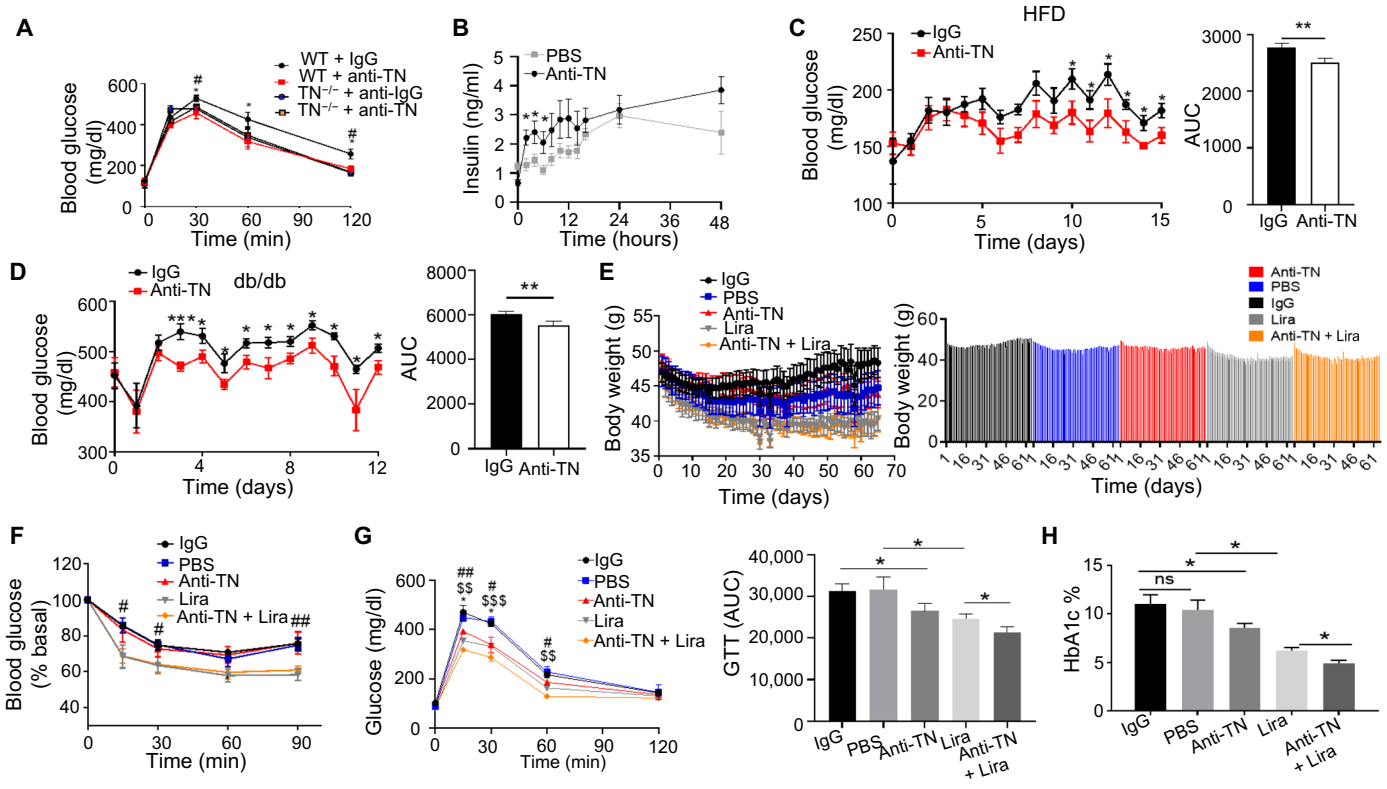

Fig. 6. TN neutralizing antibody treatment improves β cell function in mice. (**A**) IPGTT was performed after intraperitoneal injection of TN neutralizing antibody in HFD-fed (16 weeks) male mice. $^{*}P < 0.05$, when WT + IgG group was compared to WT + TN antibody. $^{\#}P < 0.05$, when $TN^{-/-}$ group was compared to WT group. (**B**) Serum insulin levels were measured in PBS- and anti-TN–treated male mice ($n = 6$ to 7 per treatment group). (**C**) Random glucose levels were measured in IgG- and anti-TN–treated male HFD mice ($n = 8$ to 9 per treatment group). (**D**) Random glucose levels were measured in IgG- and anti-TN–treated male db/db mice ($n = 10$ to 11 per treatment group). Body weight (**E**) and IPITT (**F**) in HFD-fed (16 weeks) male mice after the indicated treatments for 60 days. IPGTT (**G**) and HbA1c (**H**) levels were performed on HFD-fed (16 weeks) male mice treated with IgG, PBS, anti-TN antibody, liraglutide (Lira), or both anti-TN antibody and liraglutide ($n = 6$ each group). $^{*}P < 0.05$, when the IgG treatment group was compared to the anti-TN antibody treatment group. $^{\#}P < 0.05$, when the PBS treatment group was compared to the liraglutide treatment group. $^{\$}P < 0.05$, when the liraglutide group was compared to the anti-TN antibody plus liraglutide treatment group. Values are expressed as means ± SEM; $^{*}P < 0.05$, $^{**}P < 0.01$, and $^{***}P < 0.001$.

inhibited insulin secretion by targeting a step distal to K_{ATP} channel closure or β cell depolarization.

TN suppresses GSIS by inhibiting LTCCs in β cells

The finding that TN suppresses *KCl*-stimulated insulin release (Fig. 7E) suggested that TN may have a direct effect on free cytoplasmic Ca^{2+} levels ($[Ca^{2+}]_i$), which is a major regulator of insulin secretion. While TN had no effect on the basal $[Ca^{2+}]_i$ levels at 2.8 mM glucose, it significantly impaired *KCl* and high glucose–induced $[Ca^{2+}]_i$ increase in islets (Fig. 8A and fig. S5C). To obtain further evidence on the role of TN in regulating $[Ca^{2+}]_i$, we examined insulin secretion in purified mouse or human islets in response to a variety of Ca^{2+}-dependent secretagogues. The inhibitory effect of TN on insulin secretion in human β cells could be rescued by S-(-)-Bay K 8644, an LTCC activator, but not by L-arginine, forskolin, or sulfonylurea glibenclamide (Fig. 8B), suggesting that TN reduces insulin secretion by inhibiting LTCC activity but not by affecting membrane depolarization, adenosine 3′,5′-monophosphate (cAMP) induction, or K_{ATP} (ATP-sensitive potassium channel) closure. The Cav1.2 and Cav1.3 subtypes of the L-type channel, which are expressed in both mouse and human islets, are responsible for Ca^{2+} influx and insulin granule exocytosis in β cells (*13*). The mRNA levels of Cav1.3 have been found to be approximately 14.5 and 2.5 times higher than those of Cav1.2 in human and mouse islets (*15*, *16*), respectively. Notably, the mRNA of Cav1.3 channel encoded by the *Cacna1d* gene was significantly down-regulated by TN in human β cells (Fig. 8C). On the contrary, the mRNA levels of Cav1.3 were significantly increased in islets isolated from HFD-fed $TN^{-/-}$ mice compared to WT control mice (Fig. 8D). These data indicated a critical role of Cav1.3 channel in TN-mediated insulin regulation. We found that TN perfusion dose-dependently inhibited Ca^{2+} current in both human (Fig. 9A) and mouse β cells (Fig. 9B), suggesting TN as an endogenous LTCC inhibitor that possibly functions by inhibiting the Cav1.2-1.3 channels. This speculation was further validated by treating human embryonic kidney (HEK) 293T cells expressing Cav1.3 channel with the LTCC inhibitor nifedipine. In line with the effect of TN on LTCC in β cells, TN inhibited the ectopically expressed Cav1.3 channel in HEK293T cells in a dose-dependent manner (Fig. 9C). TN also inhibited Cav1.2 channel expressed in HEK293T cells, although to a lesser extent (fig. S5D). We also analyzed the effect of TN on the current-voltage (*I-V*) relationship in HEK293T cells expressing the Cav1.3 channel. Treating the cells with TN at a concentration of 83 μg/ml, which inhibited the calcium currents at a subsaturation level (70 to 80%), significantly reduced the peak current density of

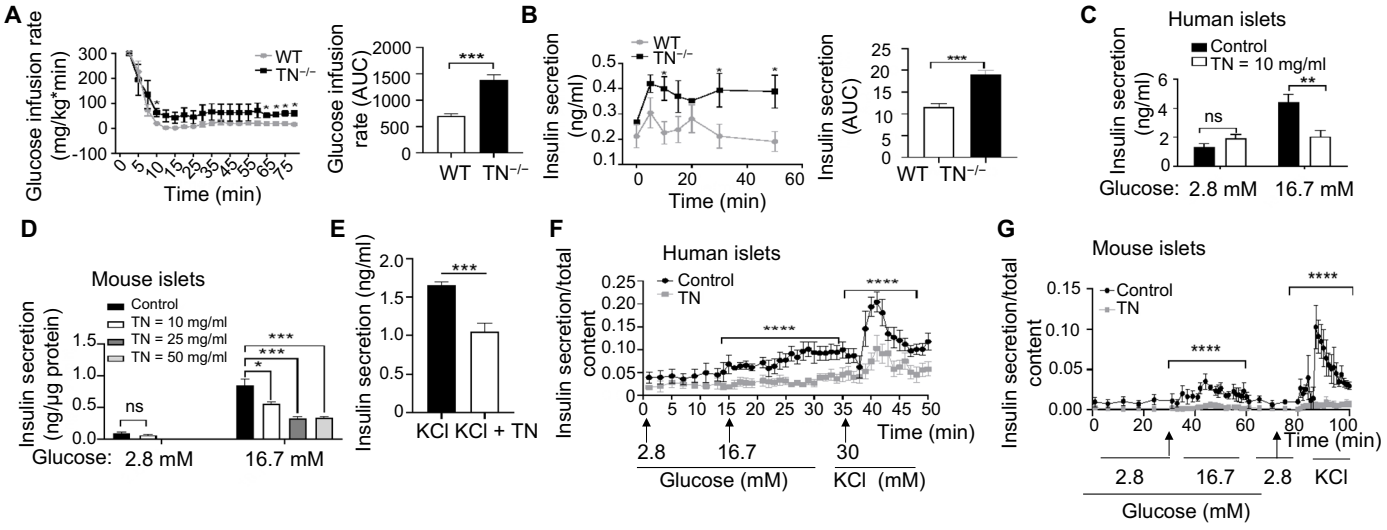

Fig. 7. TN suppresses GSIS in human and mouse β cells. (**A**) GIR in WT and TN$^{-/-}$ male mice ($n = 4$ per genotype) during hyperglycemic clamp. AUC calculations for data in (A) are shown on the right. (**B**) Plasma insulin levels in WT and TN$^{-/-}$ male mice ($n = 4$ per genotype) during hyperglycemic clamp study. AUC calculations for data in (B) are shown on the right. GSIS in human (**C**) or mouse (**D**) islets incubated with low (2.8 mM) or high (16.7 mM) glucose in the presence of different doses of TN as indicated for 30 min. Values are means ± SEM of six independent experiments, and all measurements were made in triplicate in each independent experiment. (**E**) GSIS in mouse islets incubated with 25 mM *KCl* in the presence of TN (10 μg/ml) or control vehicle for 30 min. Values are means of six independent experiments, and all measurements were made in triplicate in each independent experiment. Perfusion GSIS assays of human (**F**) and mouse (**G**) islets treated with either TN (10 μg/ml) or control vehicle. Values are means ± SEM from five independent experiments. *$P < 0.05$, **$P < 0.01$, ***$P < 0.001$, and ****$P < 0.0001$ for (A) to (G).

Cav1.3 channel (~80% at 0 mV; $P < 0.0001$; Fig. 9D), but had no significant effect on the threshold activation voltage, peak activation voltage, and reversal voltage of the channel (Fig. 9E), suggesting that TN treatment did not change the activation gating of Cav1.3. TN treatment also did not affect the steady-state activation of Cav1.3 (Fig. 9F). The inhibition is rather rapid after TN perfusion into the recording chamber, with the steady-state inhibition being reached within one sweep (5 s; Fig. 9G), indicating a direct inhibition of TN on the Cav channels.

DISCUSSION

In the current study, we reported the identification of TN as an adipose tissue–enriched secretory molecule that impairs β cell function in T2D. TN protein is highly enriched in adipose tissue, and its expression and serum levels are greatly induced in diabetic humans and mice. Administration of TN exacerbates and knockout of TN gene improves glucose tolerance in mice. Mechanistically, hyperglycemia increases the expression of TN in adipocytes via the p38 MAPK/TXNIP/thioredoxin/OCT4 signaling pathway, leading to TN suppressing GSIS in islets by blocking the LTCCs (Fig. 10). Our study provides new evidence on the possible adipo-insular axis to modulate β cell dysfunction in diabetes and suggests that inhibition of TN expression and/or neutralizing its function could be a promising therapeutic strategy for the treatment of diabetes. In addition to islets, TN-SEAP also binds to the liver and muscle, but to a much lesser extent (Fig. 4A). Nevertheless, while knockout of TN had no obvious effect on insulin sensitivity, as measured by insulin tolerance test (Fig. 5B), we cannot completely exclude the possibility that TN may have a direct effect on liver function. Further investigations will be needed to address this question.

TN mRNA is ubiquitously expressed in mouse tissues (*19*, *20*), but its protein expression appears to be more tissue restricted. Wewer *et al.* (*21*) analyzed the tissue distribution of TN mRNAs in several tissues including liver, head, trunk, skin, lung, and limbs by Northern blot and found that TN mRNA is most prominently in the lung, followed by limbs. However, no appreciable immunostaining of TN protein was detected in normal adult skeletal muscle, lung, and other organs (*21*). TN mRNA was not detected in the liver (*19*–*23*), but its protein expression was detected in human skeletal muscle by immunostaining, although Western blot did not consistently detect TN protein in muscle (*48*). In our study, we found that TN protein is predominantly expressed in human and mouse adipose tissues (Fig. 2, C and D). The anti-TN antibody detected TN protein in tissues from WT but not TN$^{-/-}$ mice (Fig. 2D), confirming the specificity of the antibody. These results demonstrate that TN is an adipose-enriched secreted molecule that may regulate β cell function via an endocrine mechanism. While TN was detected in mouse and human islets by immunohistochemistry (*35*, *36*), we found no TN mRNA in mouse islets by qPCR (fig. S1G). Consistent with this result, no TN protein expression was detected in INS-1 cells and islets (fig. S1H). We found that TN was induced in white and brown fat cells but not in muscle cells. While it is well known that muscle and BFCs are derived from the same lineage, fully differentiated muscle cells and brown adipocytes show distinct tissue distributions, unique protein expression patterns, and different characteristics. For example, BFCs are located in deeper cervical, supraclavicular, and paraspinal areas that consist of a mixture of brown and white adipocytes (*49*). They are critical for nonshivering thermogenesis via specific expression of UCP1 (*50*). Skeletal muscle cells, on the other hand, are widely distributed throughout our body and express different types of motor units, which are responsible for contraction and locomotion (*51*). The different tissue microenvironment shapes the function of the cells and orchestrate their capability in response to distinct stimuli. Thus, it is expected that brown adipocytes and skeletal muscle cells respond differently to glucose stimulation, leading to

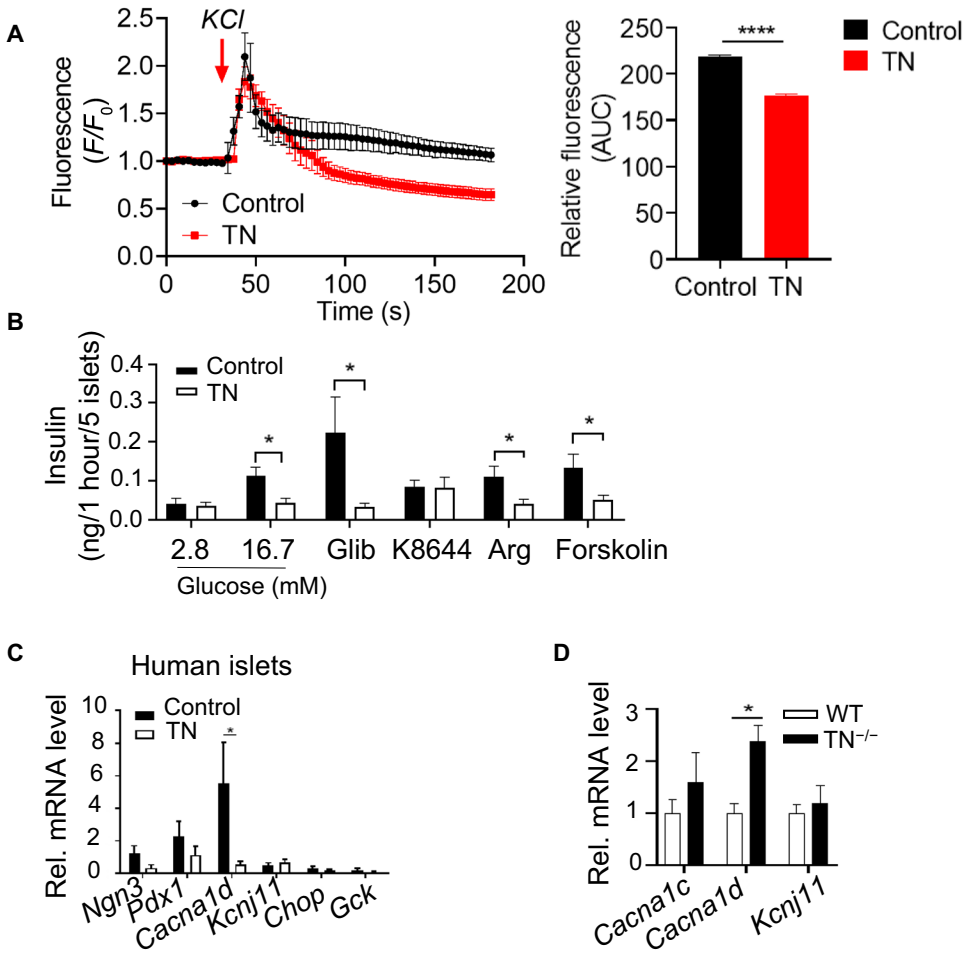

Fig. 8. TN suppresses GSIS in β cells after K_{ATP} channel. (**A**) Recordings of Fura-4 fluorescence in mouse islets after stimulation with *KCl* followed by incubation with or without TN (100 μg/ml). The sampling rate was 0.2 Hz. The histogram showed the mean F/F_0 peak at high glucose in control ($n = 6$ islets) and TN-treated islets ($n = 6$ islets). Data are means ± SEM. *$P < 0.05$. The red arrow corresponds to the time of glucose injection. (**B**) Secretagogue-stimulated insulin secretion in human isolated islets incubated with glucose (2.8 and 16.7 mM), glibenclamide (Glib; 1 mM), S-(-)-Bay K 8644 (K8644; 0.5 mM), L-arginine (Arg; 10 mM), and forskolin (5 μM) in the Krebs-Ringer bicarbonate (KRBH) buffer including 16.7 mM glucose simultaneously in the absence or presence of TN (100 μg/ml) for 1 hour. Results from eight experiments ($n = 4$ independent wells). (**C**) mRNA levels of β cell function relevant genes in human islets incubated with or without TN (10 μg/ml) for 24 hours. Data are means ± SEM from eight independent experiments, and measurements in the independent experiments were done in four independent wells. (**D**) The mRNA levels of ion channels in islets from 4-month-old HFD-fed $TN^{-/-}$ and WT control male mice were quantified by qPCR ($n = 6$ per genotype). All data are presented as means ± SEM. *$P < 0.05$ by Student's *t* test. *$P < 0.05$ and ****$P < 0.0001$.

different expression levels of TN. The serum levels of TN were correlated with diabetes but not with obesity in NGT in both male and female human subjects (Fig. 1, C and D, and fig. S1, B and C), suggesting that hyperglycemia may play a major role in promoting TN expression and/or secretion. Consistent with this view, TN expression and secretion were stimulated by glucose, but not insulin, in adipocytes (Fig. 2I and fig. S5E). Overproduction of TN inhibits insulin release, suggesting that this secretory molecule may benefit survival during evolution. For example, insulin resistance is evolutionarily well preserved, which is important for humans under specific conditions such as starvation, immune activation, and growth, when glucose is critical for different biosynthetic purposes. STZ, which induces apoptosis and necrosis in β cells, is widely used to generate diabetes animal models in diabetes research (*52*, *53*). We found that STZ treatment greatly increased serum glucose (Fig. 5D) and TN levels (Fig. 1, G and H) in mice. In addition, TN treatment increased STZ-induced reactive oxygen species (ROS) production (fig. S5F) and knockout of TN protected mice from STZ-induced diabetic symptoms and increased mouse survival (Fig. 5, D to F). These results suggest that TN may impair β cell function by increasing ROS production. Because hyperglycemia is also induced in HFD-fed mice (*54*), it is not surprising that TN levels were increased in the serum of HFD-fed mice (Fig. 1F). Obesity, at least at its early stages, often provokes hyperinsulinemia when β cells are in a compensatory phase to maintain normal blood glucose (*55*). However, impaired β cell function and reduced insulin secretion are present early during T2D development, even at the stage of impaired glucose tolerance when β cells are in a decompensated state (*56*). Our findings showed that TN expression was induced by high levels of glucose and that serum TN levels were greatly increased in patients with diabetes but not with NGT-associated early stages of obesity (Fig. 1), suggesting that TN may play a contributing role to β cell failure in MS and

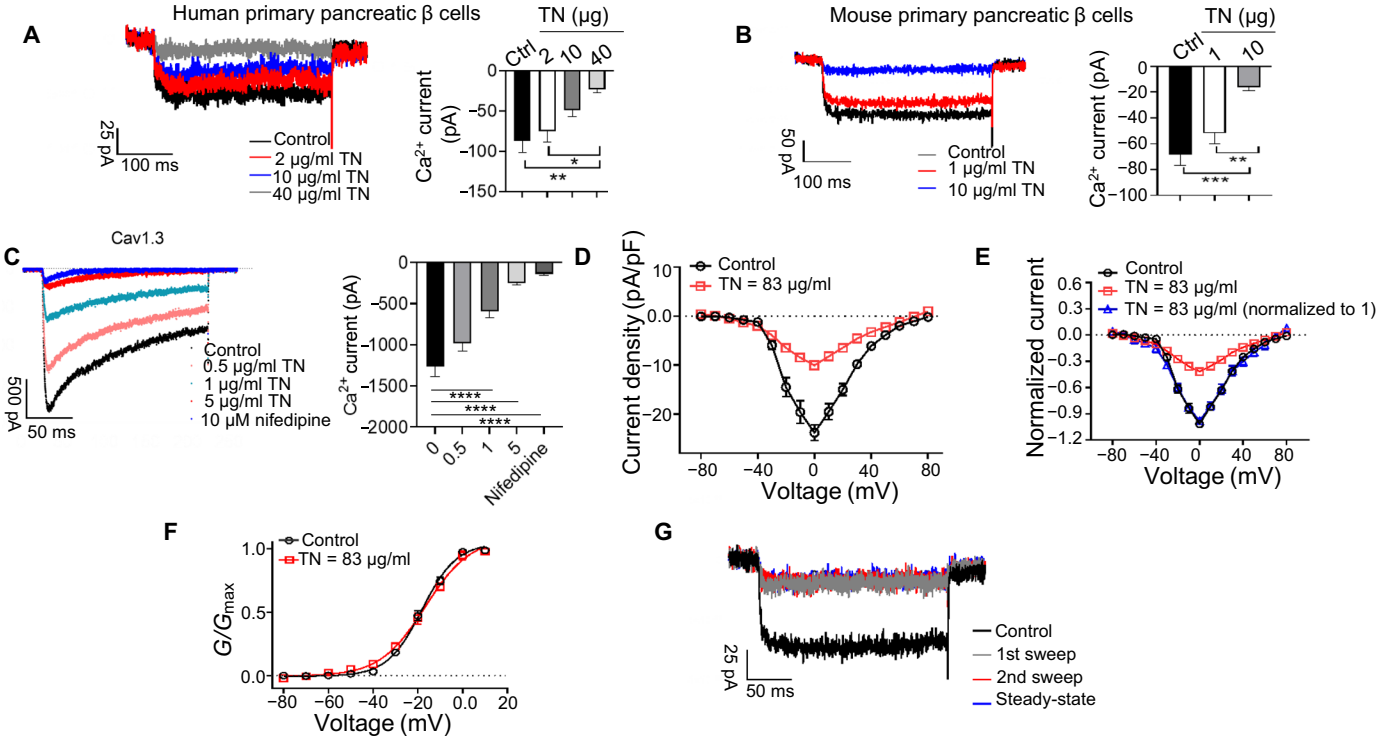

Fig. 9. TN suppresses GSIS in β cells by inhibiting LTCCs. Representative traces (left) and statistics (right) showing the dose-dependent inhibition of Cavs by TN in human primary β cells (**A**) or mouse primary β cells (**B**). Data are presented as means ± SEM of 8 to 10 cells from eight donors. (**C**) Representative traces (left) and statistics (right) showing the inhibition of Cav1.3 currents by TN in HEK293T cells ectopically expressing Cav1.3 (nifedipine was used as a positive control). (**D** and **E**) Current-voltage (*I-V*) relationship of Cavs in mouse primary pancreatic β cells in the absence or presence of TN (83 μg/ml). In (D), the currents were normalized to the cell capacitance, and in (E), the currents were normalized to the maximum current before TN treatment (black and red curves). The currents in the TN group were normalized to its own maximum current to show that the shape of *I-V* curve was not changed by TN treatment (blue curve). (**F**) Steady-state activation relationships of Cavs in mouse primary pancreatic β cells in the absence or presence of TN (83 μg/ml) (V_a is −18.12 ± −0.285 mV and −16.72 ± 0.595 mV and K_a is 7.753 ± 0.230 mV and 1.114 ± 0.455 mV for the control and TN group, respectively; $n = 6$). (**G**) Time-resolved inhibition of Cav currents in mouse primary pancreatic β cells by TN (83 μg/ml), showing that the inhibition reached steady state at the first recording sweep after TN perfusion into the chamber. Currents were recorded every 5 s. All data are presented as means ± SEM of six to eight cells. *$P < 0.05$ by Student's *t* test. *$P < 0.05$, **$P < 0.01$, ***$P < 0.001$ and ****$P < 0.0001$.

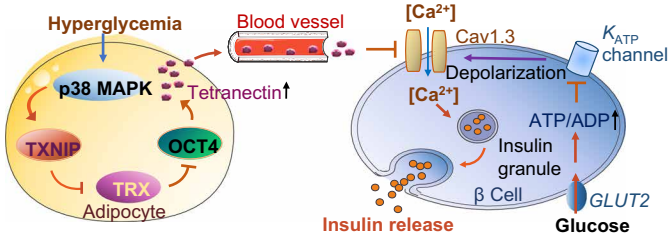

Fig. 10. A proposed mechanism by which TN suppresses GSIS in β cells. The expression and secretion of TN are up-regulated in adipose tissue under hyperglycemia condition, which is mediated by the p38 MAPK/TXNIP/thioredoxin/OCT4 pathway. Circulating TN binds to β cells and inhibits glucose-induced insulin release by blocking the LTCCs.

T2D. The mechanisms underlying the stimulatory effect of glucose on TN secretion remain unclear (*57*). Future studies will be needed to elucidate the mechanism by which hyperglycemia promotes TN expression.

We found that the expression and serum levels of TN were greatly induced in diabetic humans and mice (Fig. 1). In addition, TN expression could be induced by high levels of glucose and adipocyte differentiation (Fig. 2, E to I). While these results suggest that TN expression may be a consequence of hyperglycemia, we also found that TN administration exacerbated glucose intolerance in both NCD- and HFD-fed mice (Fig. 5, G and H). In addition, treating β cells with TN is sufficient to suppress GSIS (Fig. 7, C and D). These results suggest that TN has a direct and feedforward role in suppressing insulin secretion in β cells under hyperglycemia conditions. The pathophysiological significance for this positive feedback regulation remains unclear, but some other hyperglycemia-induced insulin secretion inhibitors such as secreted frizzled-related protein 4 (SFRP4) and retinol binding protein 4 (RBP4) have been reported to impair β cell function via a positive feedback action (*58*, *59*). Nevertheless, the findings that suppressing TN expression and neutralization of TN function improve GSIS and glucose tolerance suggest that TN may be an excellent target for diabetes therapy (Fig. 6, A and B). In support of this notion, reducing TN function by a neutralizing antibody could improve IPGTT in mice (Fig. 6, A and G). Moreover, treating obese mice with the TN neutralization antibody significantly increased the suppressing effect of liraglutide on HFD-induced hyperglycemia (Fig. 6, E to H), offering new options for the treatment of obesity-induced T2D. However, there are some studies showing that serum TN levels were inversely associated with CAD (*31*, *60*), although there is no significant correlation between TN levels and inflammatory markers such as tumor necrosis factor α (TNFα),

interleukin-6 (IL-6), IL-8, high-sensitivity C-reactive protein (hs-CRP), and monocyte chemoattractant protein 1 (MCP-1) (*61*). Further studies will be needed to determine whether TN has a causative effect on other tissues or diseases.

While it is well known that there are marked cytoarchitectural differences between human and rodent islets (*62*, *63*), our findings show that TN inhibits GSIS in both human and mouse islets (Fig. 7, C and D), demonstrating a clinical relevance of our findings. The inhibitory effect of TN on insulin secretion in human β cells could be fully rescued by the LTCC activator S-(-)-Bay K 8644, but not by the membrane depolarization agent L-arginine or the K_{ATP} channel closure inducer sulfonylurea glibenclamide (Fig. 8B). These findings indicate that the inhibitory effect of TN on insulin secretion is most likely mediated by inhibiting the LTCC activity. Consistent with this view, TN suppressed Ca^{2+} current in both human and mouse β cells as well as in HEK293T cells ectopically expressing the α1D and β3 subunits of the Cav1.3 channel (Fig. 9, A to C). The whole-cell patch-clamp results demonstrated that TN had direct and potent inhibitory effect on LTCCs in β cells. Because the patch-clamp test is acute perfusion administration, it is more likely that TN may directly inhibit calcium channels. However, how TN binds and inhibits LTCCs in pancreatic β cells is still uncertain. There are several potential possibilities by which TN regulates LTCCs. First, our data showed that TN treatment did not change the activation gating of Cav1.3 (Fig. 9, D and E) or the steady-state activation of Cav1.3 (Fig. 9F). Thus, it is possible that TN might decrease the current density by promoting the endocytosis of Cav1.3 from plasma membrane via a direct interaction with a common Ca^{2+} channel auxiliary protein or with a specific regulator of Ca^{2+} channels. Second, the plasma membrane–bound LTCCs (Cav1.2 and Cav1.3) mediate exocytosis of predocked insulin-containing secretory granules during the first phase of GSIS, which is mediated by their interaction with syntaxin-1A (*64*). Thus, TN may perturb the complex between LTCCs and syntaxin-1A or directly bind to syntaxin-1A and consequently modulate the activity of the β cell exocytotic machinery. Last, it is known that TN binds to several molecules including plasminogen (*26*), angiostatin (*65*), apolipoprotein (*27*), and heparin (*28*) as well as calcium (*66*). These results suggest a possibility that TN may interact with Ca^{2+} to block its entry into β cells via the LTCCs. Further studies will be needed to sort out these possibilities. We found that TN treatment significantly suppressed the mRNA levels of Cav1.3 channel in human islets and that knockout of TN significantly increased the mRNA levels of Cav1.3 channel in mice (Fig. 8, C and D), suggesting that, in addition to an acute inhibition, TN may regulate Cav1.3 function by suppressing Cav1.3 expression. Further studies will be needed to verify these possibilities.

In conclusion, we identify TN as a fat-enriched secreted molecule that negatively regulates GSIS in β cells in diabetes. Our study shows that TN targets β cells and inhibits insulin secretion by inhibiting LTCCs, uncovering a new mechanism underlying β cell dysfunction in diabetes. The findings that serum levels of TN are associated with diabetes in humans and that TN inhibits GSIS in human islets also suggest that reducing TN expression and/or neutralizing its function could be a promising antidiabetic therapeutic avenue to improve β cell failure.

MATERIALS AND METHODS

Study participants and study design

All participants gave written informed consent before the commencement of the study, which was approved by the Ethics Committee of Second Xiangya Hospital of the Central South University (CSU) (protocol MSRC2016LF). For proteomic profiling experiments, serum samples were collected from 22 age-matched male adult human subjects, including 10 healthy subjects, 7 obese NGT (without hypertension, hyperlipidemia, and hyperglycemia), and 5 human subjects with MS (table S1). Obese patients were newly diagnosed, and individuals were classified as underweight (<18.5 kg/m^2), normal (18.5 to 24.0 kg/m^2), overweight (24.0 to 27.9 kg/m^2), or obese (≥28.0 kg/m^2) according to Chinese criteria. The International Diabetes Federation defined MS as central obesity (waist circumference ≥ 90 cm in Chinese men) in addition to any two of the following: elevated triglyceride (TG) levels (>1.7 mM or specific treatment for this lipid abnormality), low high-density lipoprotein cholesterol (HDL) levels (<1.03 mM in men or specific treatment for this lipid abnormality), hypertension (systolic, >130 mmHg; diastolic, >85 mmHg; or treatment of previously diagnosed hypertension), and elevated fasting plasma glucose [fasting blood glucose (FPG), >5.6 mM or previously diagnosed T2D] (*67*). The body mass index (BMI) was calculated as weight (kg)/height (m^2). Other parameters such as age, gender, waist, hip, systolic blood pressure, and diastolic blood pressure were recorded by physician assistants. Fasting venous blood samples were tested for FPG, TG, total cholesterol, HDL, and low-density lipoprotein cholesterol (LDL). Two-hour postprandial venous blood samples were tested for 2-hour postprandial glucose (2hPG). The exclusion criteria for all the participations were the following: frequent use of anti-inflammatory drugs or corticosteroid medications; T1D; secondary diabetes; inflammation, infectious diseases, or other autoimmune disorders; pregnancy; and malignant diseases. The normal controls and obesity group also excluded any patients with a history of T2D, hypertension, and hyperlipidemia. Immediately after collection, blood samples were allowed to clot at room temperature for 4 hours, and the serum samples were collected and centrifuged at 3000 rpm for 15 min. To remove lipids, the serum samples were mixed with 250 μl of buffer containing 100 mM NaCl and 10 mM Hepes (pH 7.4) and filtered through 0.22-μm filters by spinning at 10,000*g* for 30 min. The lipid-free serum sample (260 μl) was mixed with 182 μl of cold ethanol, rested at 4°C for 1 hour, and subjected to centrifugal separation at 16,000*g* for 45 min. Last, the solutions and precipitations were separated via the above steps, and the serum samples were stored at −20°C after lyophilization.

For Western blot experiments, serum samples were collected from a new group of age- and sex-matched human adults, including 24 healthy subjects (BMI < 24 kg/m^2), 24 obese NGT (BMI ≥ 28 kg/m^2, FPG < 7.0 mM, and HbAc1 < 6.5%), and 24 T2D subjects (BMI ≥ 28 kg/m^2, FPG ≥ 7.0 mM, and HbAc1 ≥ 6.5%) (tables S2 and S3). Diagnostic criteria of T2D were (i) typical history of hyperglycemia according to American Diabetes Association criteria (*68*), (ii) negative for islet autoantibodies, and (iii) not requiring immediate insulin treatment. T2D was diagnosed by meeting one of the following conditions: FPG ≥ 7.0 mM, 2hPG ≥ 11.1 mM, HbAc1 ≥ 48 mM (6.5%), and random plasma glucose ≥ 11.1 mM. The exclusion criteria for all the participations were the same as those for the proteomic profiling experiment.

Human pancreases were obtained from deceased nondiabetic donors by the Department of Urological Organ/Liver Transplantation team at the Second Xiangya Hospital of the CSU. Human islets were isolated by collagenase P (Sigma-Aldrich, C9263) digestion of the pancreas according to the procedures described (*69*). Human pancreases were trimmed after carefully removing the surrounding

fat tissue, lymph nodes, vessels, and membranes. Pancreatic ducts were cannulated and inflated with a 5-ml syringe and Hanks' balanced salt solution (HBSS) containing collagenase P (1 mg/ml) injected through the pancreatic duct. Two milliliters of collagenase solution was used per each milligram of pancreas. The pancreas was removed and incubated at 37°C for about 20 to 30 min in 50-ml centrifuge tube to allow complete digestion. The tubes were placed in an ice bath, and digestion was stopped by the addition of HBSS, followed by rinsing the pancreases with HBSS three times. Islets were collected using a pipette under a stereoscopic microscope and maintained at 37°C in CMRL 1066 medium (Gibco) supplemented with fetal bovine serum (FBS) [10% (v/v); Gibco], glutamine (2 mM; Gibco), and penicillin-streptomycin (100 U/ml, 0.1 mg/ml; Gibco). Table S5 presents the basic information for human pancreas.

Proteomic profiling

The lyophilized human serum samples were dissolved individually in 200 μl of 6 M GuHCl (guanidine hydrochloride) separately. The solution (45 μl) containing 300 μg of proteins was reduced by adding 2 μl of 1 M dithiothreitol (DTT) and incubated at 37°C for 2.5 hours. Then, 10 μl of 50 mM iodoacetamide was added to the solution, and the mixture was incubated in the dark for 40 min at room temperature. After the reaction, the samples were centrifuged at 10,000*g* for 20 min using a Centricon YM-50 column (Millipore, Bedford, CA), and the concentrated samples (~30 μl) were digested with 2 μg of trypsin (Promega, Madison, WI) at 37°C for 20 hours. The digested peptides were centrifuged at 10,000*g* for 10 min, and the clarified supernatants were stored at −80°C for further analysis with mass spectrometry. Peptides were subjected to two-dimensional (2D) liquid chromatography–tandem mass spectrometry (LC-MS/MS) separation, which was composed of an SCX (Strong Cation Exchange) column [320 μm inside diameter (id), 100 mm length; Column Technology], two C18 RP (Reversed-Phase) trap columns (Agilent Technologies), and one C18 RP capillary column (75 μm id, 100 mm length; Column Technology), coupled with two Agilent 1100 high-performance LC pumps (Agilent Technologies). The flow rate of SCX and RP trap was 3 μl/min, and the flow rate of RP was 2 μl/min. We fractionated the sample into 10 fractions by SCX, as described in Zhou *et al.*'s work (*70*). 2D LC was further interfaced to a linear ion trap mass spectrometer (LTQ). The mass spectral data were acquired on a linear ion trap mass spectrometer (LTQ) (Thermo Fisher Scientific, San Jose, CA) equipped with an electrospray interface operated in positive ion mode. The column effluent was directed into the LTQ mass analyzer. The electrospray ionization conditions were the following: 3.0 kV for the spray voltage and 170°C for the capillary temperature. The mass spectrometer was set so that each full mass spectroscopy scan was followed by the 10 most intense peptide ions for MS/MS with charge $\geq$ +2 with the following dynamic exclusion settings: repeat counts, 1; repeat duration, 30 s; exclusion duration, 180 s. All data files were created using Bioworks 3.1, with precursor mass tolerance of 1.4 Da, threshold of 100, and minimum ion count of 15. The acquired mass spectrometry spectra were searched against the Human International Protein Index protein sequence database (version 3.07; www.ebi.ac.uk/IPI) combined with sequences of real protein and reverse sequences of proteins by using the TurboSEQUEST program in the Bioworks 3.1 software suite, with a mass tolerance of 3.0 Da. All cysteine residues were searched as carboxamidomethycystein (+57.02 Da). Up to one internal cleavage site was allowed for tryptic searches. All output results were combined using the in-house software named Buildummary to delete the redundant data. Searches were conducted against the Human International Protein Index protein sequence database to control the false discovery rate at 2.5%, and all spectral peptide count had a DCn score of at least 0.1. The proteins identified by two or more peptide counts in either nondiabetic or diabetic serum were used to the following bioinformatics analysis.

RNA sequencing and data analysis

Total RNA was prepared from differentiated adipocytes using the RNeasy Mini Kit (QIAGEN) according to the manufacturer's instructions. RNA concentration and integrity were then controlled on a Bioanalyzer system (Agilent), and only RNA samples with RIN (RNA integrity number) values of >7 were used for downstream applications. Library construction and sequencing was outsourced to IGA Technology Services Srl. Libraries were constructed using the Nextera Library Prep Kit (Illumina) according to the manufacturer's instructions and sequenced on an Illumina HiSeq 2500 at 75–base pair single ended, with a minimum output of 40 million reads per sample. Read mapping and differential expression analysis was performed using the AIR (Artificial Intelligence RNA-Seq) software from Sequentia Biotech with the following pipeline: BBDuk (reads trimming; https://jgi.doe.gov/data-and-tools/software-tools/bbtools/bb-tools-user-guide/bbduk-guide/), STAR [reads mapping to the human genome GRCh38 (Ensembl); https://github.com/alexdobin/STAR], featureCounts (gene expression quantification; http://subread.sourceforge.net/featureCounts.html), and EdgeR (differential gene expression; www.bioconductor.org/packages/devel/bioc/html/edgeR.html). The expression level of each gene was calculated using the fragments per kilobase of transcript per million (FPKM) base pair sequenced method. To identify the DEGs between two groups (three biological replicates per group), Cuffdiff was used. Genes with a fold change of $\geq$2 and a false discovery rate of <0.05 were identified as significant DEGs. To comprehend the functions of these DEGs, GO functional enrichment and the Kyoto Encyclopedia of Genes and Genomes (KEGG) pathway analysis were performed.

Culture of primary human preadipocytes and adipocytes

Abdominal WAT was obtained from nondiabetic patients during abdominoplasty. Approval was obtained from the Ethics Committee of Second Xiangya Hospital of the CSU (protocol MSRC2016LF). The isolation of adipocyte and SVF cells was performed as described (*71*).

Human preadipocytes were maintained in Dulbecco's modified Eagle's medium (DMEM) containing 10% FBS, penicillin (100 U/ml), and streptomycin (50 μg/ml) at 37°C in 5% CO_2. To induce differentiation, confluent human preadipocytes (day 0) were subsequently cultured in serum-free DMEM containing 50 nM insulin, 100 nM dexamethasone, 0.5 mM 3-isobutyl-1-methylxanthine, and 100 μM rosiglitazone. The medium was changed every 2 days for the first 4 days. Thereafter, the medium was replaced by serum-free DMEM containing 50 nM insulin and 100 nM dexamethasone, which was changed every 2 days until lipid droplets had accumulated (days 14 to 17). Seventeen days after the induction of differentiation, more than 90% of the cells had acquired the adipocyte phenotype, the cells used for the experiments.

Animal studies

All procedures for animal use were in accordance with the Animal Care and Use Committee of the Second Xiangya Hospital, CSU or

the Animal Care and Use Committee of University of Texas Health at San Antonio (UTHSA). Institutional Regulatory Board and/or Institutional Animal Care and Use Committee guidelines were followed with animal subjects. The $TN^{-/-}$ mice in C57BL/6J background were obtained from the Shanghai Research Center for Model Organisms and were described previously (*30*). $TN^{-/-}$ mice can be provided by E. Wang pending a scientific review of the request and a completed material transfer agreement. Requests for $TN^{-/-}$ mice should be submitted to E. Wang. TN whole-body knockout ($TN^{-/-}$) mice were maintained on a C57BL/6J background. Heterozygous $TN^{+/-}$ mice were crossed to produce WT ($TN^{+/+}$) and knockout ($TN^{-/-}$) mice according to the Mendelian law. In our studies, control animals were derived from the same cross and not from parallel breeding of WT animals to ensure as close a genetic match as possible to the test animals. $TN^{+/-}$ mice are phenotypically similar to $TN^{+/+}$ mice (Fig. 5A). All mice were housed in a specific pathogen–free environment with a 12-hour light/12-hour dark cycle at either the Animal Care Center in the Second Xiangya Hospital of the CSU or the Animal Facility at the UTHSA. The mice were all in C57BL/6J background and had free access to food and water. Mice were fed an NCD containing 19% protein, 5% fat, and 5% fiber (Hunan Silaike Jingda Laboratory Animal Co. Ltd.) or an HFD containing 20% protein, 60% fat, and 20% carbohydrate (D12492, Research Diets Inc.) starting at 6 weeks of age.

Body weight and body composition measurement

Body weight and food intake were measured weekly at the same time points from week 6 and onward. Mouse body composition (fat mass and lean mass) was determined using an MQ Minispec 7.5 HZ Live Mice analyzer (MinispecLF50, BRUKER Optik GmbH, Germany).

TN binding assay

TN binding assay was performed according to the procedure as described previously (*72*). To identify the target tissue(s) of TN, we generated a plasmid encoding a fusion protein in which the *TN* gene was fused to the cDNA encoding the secreted human placental alkaline phosphatase (SEAP-TN). Plasmids encoding SEAP or SEAP-TN were expressed in HEK293T cells, and cell culture medium containing the secreted SEAP or SEAP-TN was collected. TN binding assay was performed by incubating frozen mouse tissue sections with SEAP- or SEAP-TN–containing cell culture medium. For competition binding assays, frozen tissue slices were preincubated for 1 hour with His-TN (20 mg/ml), followed by incubation with SEAP-TN cultured medium for 1 to 2 hours at room temperature.

Generation and purification of recombinant TN and green fluorescent protein

The TN cDNAs were amplified from human or mouse WAT by PCR and cloned into the pcDNA 3.1/myc-His B vector (Invitrogen/Thermo Fisher Scientific). The expression of the recombinant TN fused with a secretory peptide sequence (to assist secretion) and an N-terminal 6×His tag at its N terminus was produced in HEK293T cells. His-tagged green fluorescent protein (GFP) purified from HEK293T cells was used as a control. The medium was collected, and cells in the medium were removed by centrifugation. The clarified medium was sterile-filtered, concentrated, and buffer-exchanged into a nickel-binding buffer [50 mM $NaPO_4$ (pH 7.4), 500 mM NaCl, and 25 mM imidazole] by using an ÄKTA FPLC (Fast protein liquid chromatography) system. TN was purified from this solution via nickel-affinity chromatography using a HisTrap excel column (GE Healthcare) followed by size exclusion chromatography using an analytical Superdex 200 column (GE Healthcare) equilibrated with phosphate-buffered saline (PBS) containing 10% glycerol. The purified proteins were of high purity (>90%), as judged by silver staining (fig. S6A), LC (fig. S6, B and C), and mass spectrometry (fig. S6D). The identity of TN protein was confirmed by silver staining and Western blotting (fig. S6A). The purified TN was able to regulate insulin secretion, as demonstrated by in vivo and in vitro experiments (Figs. 5I and 7, C to G), suggesting that the protein structure is intact. Recombinant TN was expressed in mammalian cells, which do not produce endotoxins. For some experiments including the islet perfusion and in vivo experiments, purified TN proteins from Sino Biological Inc. (50700-M08H), which are >95% pure, were used. The commercially obtained TN showed similar effect to that of the homemade TN, confirming the specific effects of the proteins.

Plasma TN half-life measurement

His-tagged and mammalian cell–expressed TN was obtained from Sino Biological Inc. (catalog no. 50700-M08H). TN (~1 mg/kg) was injected intraperitoneally into WT C57/BL6 mice. Blood was drawn before injection (baseline) and at 0.25, 0.5, 1, 2, 4, 8, 16, 32, 48, 60, and 72 hours after injection. The plasma concentration of TN was determined by Western blots. The half-life of TN protein was calculated using GraphPad Prism 6 software.

Generation of anti-TN antibody

The TN antibody was generated in female New Zealand white rabbits at Covance Inc. (Princeton, NJ, USA) using recombinant fragment corresponding to mouse TN amino acids 86 to 144 expressed in *Escherichia coli* following standard procedures. Blood samples were collected in 3-week cycles of immunization and bleeding, and the antibody titers were determined by indirect TN ELISA. Total IgGs were purified from the serum using protein A affinity column. Briefly, rabbit serum was prebuffered with PBS and slowly loaded onto the protein A column to allow sufficient binding of IgGs. After washing with 1× PBS to remove unbound serum components, the IgGs were eluted with acidic buffer [0.1 M glycine-HCl (pH 2.8)] and then immediately dialyzed into 1× PBS buffer at 4°C overnight. The plasma concentration and the half-life of the anti-TN antibody were determined by a homemade ELISA kit (fig. S5G).

Injection of TN neutralizing antibody into mice

HFD-fed 16-week-old male $TN^{-/-}$ mice and their WT littermates were injected daily with TN antibody protein (2 mg/kg, intraperitoneally). Control mice were injected intraperitoneally with an identical volume of IgG. Treated animals were fasted 12 hours before the glucose tolerance test.

The combination of liraglutide and anti-TN neutralizing antibody study

The mice fed an HFD for 16 weeks received daily intraperitoneal injections of either 0.9% (w/v) sodium chloride, liraglutide (0.1 mg/kg), anti-TN polyclonal antibodies (pAbs) (2 mg/kg), IgG (2 mg/kg), or both liraglutide and anti-TN pAbs for 60 days. Mouse body weights were measured every day throughout the study. IPGTT and IPITT (Intraperitoneal Insulin Tolerance Test) were measured as described previously. Blood samples were used directly for the measurement of HbA1c (Jiancheng Biotechnology).

IPGTT, IPITT, and GSIS assays

IPGTT and IPITT were performed as described in our previous experiments (*73*). For some experiments, a single dose of recombinant TN (1 mg/kg) was intraperitoneally injected into 16- and 4-hour fasted mice before IPGTT and IPITT experiments, respectively. For a long-term study, recombinant TN was intraperitoneally injected into 4-month-old C57BL/6J mice at a single dosage of 1 mg/kg every day for 2 weeks before IPGTT experiments. For liraglutide study, WT and $TN^{-/-}$ mice fed an HFD for 16 weeks were dosed subcutaneously with liraglutide (0.2 mg/kg) (Novo Nordisk) or vehicle 2 hours before IPGTT experiments (2 g/kg).

For GSIS ex vivo test, freshly isolated human or mouse islets were incubated overnight in RPMI 1640 medium (Gibco) containing 10% FBS (Gibco) and penicillin-streptomycin (100 U/ml) (Gibco) at 37°C in the cell culture incubator. The islets were then transferred to a Hepes-balanced Krebs-Ringer bicarbonate buffer (KRBH) (pH 7.4) containing 115 mM NaCl, 5 mM *KCl*, 2.5 mM $CaCl_2$, 1 mM $MgCl_2$, 24 mM $NaHCO_3$, 25 mM Hepes, bovine serum albumin (BSA) (1 mg/ml), and 2.8 mM glucose and incubated for 2 hours. Subsequently, the islets (five islets per well) were divided into four groups and incubated for 30 min in KRBH buffer containing 2.8 or 16.7 mM glucose, with or without recombinant TN. To measure the islet insulin content, islets were handpicked and lysed in 0.5 ml of acid ethanol (1.5 ml of HCl in 100 ml of 70% ethanol). The supernatant insulin levels were determined using a mouse insulin ELISA kit (Alpco Diagnostics, Salem, NH) according to the manufacturer's instructions.

For perifusion experiments, batches of 100 human or mouse islets were placed in parallel perifusion chambers at 37°C and perifused at a flow rate of 1 ml/min with a KRBH containing 0.5% BSA. Islets were first equilibrated for 20 or 30 min in KRBH supplemented with 2.8 mM glucose and then stimulated during 20- or 30-min periods in high glucose concentrations (16.7 mM) with or without TN as indicated. Fractions were collected every minute. At the end of each perifusion, islets were pelleted by centrifugation and lysed in acid ethanol for assessment of insulin content by RIA (Radioimmunoassay). Results are presented as insulin secreted (ng/ml) per minute normalized to islet insulin content.

Hyperglycemic clamp experiments

Hyperglycemic clamp studies were performed according to the procedure as described in our previous study (*73*). Hyperglycemic clamps were performed in conscious male $TN^{-/-}$ mice and their WT littermates at 2 to 3 months of age ($n = 4$ per group). Briefly, mice were fasted overnight and anesthetized by an intraperitoneal injection of ketamine (body weight of 100 mg/kg) and xylazine (body weight of 10 mg/kg). An indwelling catheter was inserted in the right internal jugular vein 4 to 5 days before the clamp experiments. Mice were housed in individual cages and monitored for postoperative recovery and weight gain. After overnight fast, a 2-hour hyperglycemic clamp experiment was conducted in conscious mice with a variable infusion of 20% glucose to raise and maintain plasma glucose concentration at ~300 mg/dl. Blood samples (40 μl) were collected at 5- to 10-min intervals for the measurement of plasma glucose and insulin levels.

STZ treatments

For STZ treatments, 8-week-old mice were injected intraperitoneally with freshly prepared STZ (45 mg/kg) (Sigma-Aldrich, S0130) in 0.1 M citrate buffer (pH 4.5) or equal volumes of citrate buffer daily for five consecutive days. Three days after the final injection, the mice were fasted overnight and subjected to IPGTT. For hyperglycemia measurements, the random blood glucose levels of an additional cohort of mice were monitored every other day until day 60. Mice were euthanized by cervical dislocation, and tissues were collected on day 100 when there are differences in survival rates in two groups of mice. The development of diabetes was characterized as two random consecutive blood glucose readings over 250 mg/dl (*74*).

Calcium imaging

Islets were grown on poly-D-lysine (Sigma-Aldrich, P4832)–coated glass-bottom dishes overnight and incubated for 40 min at 37°C in 25 mM Hepes buffer (pH 7.4) containing 125 mM NaCl, 5.9 mM KCl, 2.56 mM $CaCl_2$, 1.2 mM $MgCl_2$, 3 mM glucose, 1% BSA, and Fluo-4 AM (3 M; Dojindo Laboratories, F312). Islets were stimulated with 16.7 mM glucose or 25 mM *KCl* after treatment with or without TN. Fluorescence imaging experiments were performed with a laser scanning confocal microscope coupled to an inverted microscope (LSM780, Zeiss), excitation wavelength of 488 nm, and emission at >510 nm. The collected data were exported and analyzed as F/F_0 ratios, where F_0 is the initial fluorescence intensity and F is the fluorescence signal recorded at an individual time point during the experiment.

Electrophysiological recordings

Whole-cell Ca^{2+} currents in the voltage-clamp mode were recorded by the patch-clamp technique according to the procedure described in a previous study (*75*). Briefly, primary pancreatic β cells that were dispersed and cultured on glass coverslips were placed into the perfusion chamber mounted on the stage of an inverted phase-contrast microscope (Olympus). Cells were washed with bath solution in the chamber for 3 to 5 min before starting an experiment. TN was applied by a pipet located close to the recording cell, and patch pipettes were pulled from borosilicate glass capillaries with filament, with a tip resistance of 2 to 3 megohms when filled with pipette solution. Whole-cell ionic currents were recorded with a HEKA EPC-10 USB patch-clamp system (HEKA Elektronik, Ludwigshafen, Germany) and analyzed by Igo Pro-6.00, Prism (GraphPad Software, La Jolla, CA, USA). At the beginning of each experiment, the junctional potential between pipette solution and bath solution was electronically adjusted to zero. Capacitive transients were automatically compensated by C-fast and C-slow. No leakage subtraction was performed for the original recordings, and all cells with visible changes in leakage currents during the study were excluded from further analysis.

In electrophysiology recordings, the human or mouse β cells were identified by analyzing the steady-state inactivation relationship of the endogenously expressed voltage-gated sodium channels, as suggested by a previous study (*76*). Briefly, the Na^+ channels in β cells were supersensitive to conditional voltage change, with the channel availability in +10-mV test pulse increasing approximately ninefold when shifting the conditional pulse from −70 to −120 mV in a standard two-pulse protocol.

HEK293T cells were transfected with a plasmid encoding GFP (pEGFP-N1) together with plasmids encoding Cav1.3e (α1D subunits) [8a,11,31b, Δ32,42a] (catalog no. 49333, Addgene) or Cav1.2 (α1C subunits) (catalog no. 26572, Addgene), rCavβ3 (β3 subunits) (catalog no. 26574, Addgene), and rCavα2δ1 (catalog no. 26575, Addgene) using Lipofectamine 2000 (Thermo Fisher Scientific,

Waltham, MA, USA). The green fluorescence was used for visualizing individual transfected cells. The transfected cells were seeded onto a glass coverslip (Thermo Fisher Scientific) 6 hours after transfection, and patch-clamp experiments were performed 24 hours thereafter (*75*).

Cav1.3 currents were recorded by a 200-ms step pulse ranging from −80 to +40 mV, with a holding potential of −70 mV. The pipette solution for Ca^{2+} currents of human β cells (*58*) was composed of 125 mM Cs-glutamate, 10 mM CsCl, 10 mM NaCl, 1 mM $MgCl_2$, 5 mM Hepes, 3 mM ATP, 0.1 mM cAMP, and 0.05 mM EGTA (pH 7.2 with CsOH). The bath solution for Ca^{2+} currents of human β cells consisted of 138 mM NaCl, 20 mM TEACl, 5.6 mM KCl, 2.6 mM $CaCl_2$, 1.2 mM $MgCl_2$, 5 mM Hepes, and 5 mM glucose (pH 7.4 with NaOH). The pipette solution for Ca^{2+} currents of mouse β cells (*75*) contained 120 mM CsCl, 20 mM TEACl, 1 mM $MgCl_2$, 10 mM Hepes, 5 mM EGTA, 5 mM MgATP, and 0.3 mM Na_2GTP (pH 7.2), whereas the bath solution for Ca^{2+} currents of mouse β cells included 100 mM NaCl, 20 mM TEACl, 20 mM $BaCl_2$, 1 mM $MgCl_2$, 10 mM Hepes, and 10 mM glucose (pH 7.4). For Ca^{2+} current recording, a gigohm seal was made in normal extracellular high-Na^+ solution. After formation of whole-cell mode, Ba^{2+}-carried Ca^{2+} currents were recorded in a Ba^{2+}-containing bath solution. The osmolarity of the recording solutions was adjusted to 290 mOsmol/liter and pH to 7.2 to 7.4. Cells were continuously perifused with the bath solution containing the tested chemicals at the desired final concentrations. All chemicals were products of Sigma-Aldrich (St. Louis, MO, USA) and dissolved in sterile double-distilled H_2O. All experiments were at room temperature.

In vitro siRNA treatment

Primary SVF cells at about 90% confluency were transfected with siRNAs. siRNAs targeting human *Txnip* (siRNA#1: CUCCCUGCUAUAUGGAUGUTT) and control siRNA were purchased from RiboBio (Guangzhou, China). siRNA (100 nM) was transfected into SVF using the Lipofectamine 3000 Transfection Reagent (Invitrogen) according to the manufacturer's instruction. qPCR analysis was used to quantify transfection efficiency.

RNA analysis

Total RNAs were isolated from TRIzol (Life Technology)–treated cells or tissues according to the manufacturer's suggested protocol. RNA concentration was determined using UV-Vis Spectrophotometer Q5000. qPCRs were performed using the SYBR green mix (Roche) and quantitated using Applied Biosystems 7900 HT sequence detection system. Duplicated runs of each sample were normalized to β-actin to determine relative expression levels. Primer sequences were provided in tables S6 and S7.

Immunofluorescence, TUNEL assay, and immunoblotting analyses

Mouse pancreases were cut into 10-μm sections systematically through the pancreatic head to tail axis, and sections were selected between every 200 μm. Eight sections per mouse were picked. The immunofluorescence (IF) experiments were carried out essentially as previously described (*73*) with some modifications. Briefly, pancreases obtained from 16-week-old male $TN^{-/-}$ mice and their WT littermates, cleared of fat and spleen, were weighted and fixed in ice-cold 4% paraformaldehyde (Electron Microscopy Sciences, Fort Washington, PA). The fixed tissues were embedded in O.C.T. (optimal cutting temperature) compound (Sakura, 4583) and cut into 10-μm sections using a cryostat or a microtome (LEICA, CM 1950). The slices were rehydrated, permeabilized, and stained with specific antibodies: insulin (1:500; Sigma-Aldrich, I2018), glucagon (1:500; Cell Signaling Technology, 2760S), Ki67 (1:500; Abcam, ab16667), and Ngn3 (1:50; Santa Cruz Biotechnology, sc-136002). The cell nuclei were identified by 4′,6-diamidino-2-phenylindole (DAPI) staining. Fluorescence signals were detected with anti-rabbit IgG conjugated with 488 (1:300; Cell Signaling Technology, 4412S) and anti-mouse IgG conjugated with 647 (1:300; Cell Signaling Technology, 4410S) observed with an Olympus inverted microscope (IX71) and captured with a Sport II digital camera. All insulin-positive β cell clusters (islets) were loosely traced, and the insulin immunoreactive areas were determined by using the threshold option. Total tissue areas were quantified with the threshold option to select the stained areas from unstained areas (white space). The islets area (in square micrometers) and the area of each section were analyzed by the ImageJ software. Four to eight sections of each pancreas were covered by accumulating images from eight nonoverlapping fields of 1.5×10^6 μm^2. Analyses of β cell area and size were performed by using ImageJ software or the Image-Pro Plus (version 5.0) software (Media Cybernetics Inc.). β cell mass was calculated by insulin-positive area/total pancreas area times pancreas weight. α Cell mass was calculated by glucagon-positive area/total pancreas area times pancreas weight. The percentage of Ki67 or Ngn3 and the ratio of insulin double-positive nuclei to total insulin-positive nuclei were determined as proliferation probability or dedifferentiation probability.

Frozen sections of the pancreas were labeled with an in situ cell death detection kit (Roche, 11684817910) and insulin antibody, and HFD-induced apoptosis was determined by IF using an Olympus inverted microscope (IX71) and captured with a Sport II digital camera. Six mice per group were used for TUNEL assays. More than 2500 insulin-positive cells were counted per mice. Apoptosis was calculated by TUNEL and insulin double-positive nuclei to total insulin-positive nuclei.

TN in serum and tissues was determined by Western blot using a homemade mouse anti-TN pAb (1:1000) or rabbit monoclonal to TN (1:1000; Abcam, ab108999), respectively. The monoclonal anti-TN antibody recognizes both human and murine TN proteins, and the specificity was verified by the manufacturer. Human or mouse serum TN levels were determined using a human TN ELISA kit (catalog no. ELH-CLEC#B-1, RayBiotech) or mouse TN ELISA kit (catalog no. H624-1-2, NJJCBIO), respectively, according to the manufacturer's instructions. The specificity of the TN antibody was confirmed by the lack of the TN signal in the tissues and serum of $TN^{-/-}$ mice (Fig. 2D and fig. S3A). Other antibodies used in immunoblotting experiments were anti–β-actin (1:5000; Sigma-Aldrich, A3854), rabbit polyclonal anti-MAPK [extracellular signal–regulated kinase 1/2 (ERK1/2)] (1:1000; homemade), rabbit polyclonal anti-adiponectin (1:5000; homemade), rabbit polyclonal anti-UCP1 (1:1000; Sigma-Aldrich, U6382), mouse monoclonal anti–β-tubulin (1:1000; Sigma-Aldrich, T4026), mouse monoclonal anti-Myc (1:5000; Abmart, M20002), anti-rabbit IgG horseradish peroxidase (HRP) conjugate (1:5000; Promega, W4011), anti-mouse IgG HRP conjugate (1:5000; Promega, W4021), and transferrin (Proteintech, 17435-1-AP).

Intracellular ROS detection

MIN6 cells were incubated with TN (100 μg/ml) for 8 hours together with various concentrations of STZ (0 and 10 mM) for 16 hours, and then DCFH-DA (2′,7′-Dichlorodihydrofluorescein diacetate) was

added at a concentration of 10 μM. After cocultured for 30 min, the cells were washed with PBS and observed using an Olympus inverted microscope (IX71) and captured with a Sport II digital camera.

Statistics

The GO figure was plotted by the online program DAVID Bioinformatics Resources 6.7 (https://david.ncifcrf.gov/). Statistically significantly enriched pathways and diseases of DEGs were identified by KOBAS 3.0 (http://bioinfo.org/kobas). The values used to cluster analysis were adjusted by mean centering and normalizing of genes and then clustered by a city-block distance–based complete linkage hierarchical method. Heatmaps were generated by Gene Cluster 3.0.

Data are presented as the mean ± SEM for normally distributed parameters or as the median (25th to 75th percentile) for non-normally distributed parameters. Differences between groups for normally distributed variables were tested using *t* test [analysis of variance (ANOVA)], except whereas indicated by ANOVA. Associations between HbA1c and TN expression were analyzed by Spearman's rank correlation and linear regression and corrected for age, sex, and BMI. The type of test used is indicated in the figure legends. For statistical analysis, SPSS version 20.0 (IBM Corporation, Chicago, IL) and GraphPad Prism 8 (GraphPad Software, San Diego, CA) software were used. *P* value below 0.05 was considered statistically significant. Beta values are from the linear model and denote effect. $^{*}P < 0.05$, $^{**}P < 0.01$, and $^{***}P < 0.001$, and $^{****}P < 0.0001$.

SUPPLEMENTARY MATERIALS

Supplementary material for this article is available at https://science.org/doi/10.1126/sciadv.abq1799

View/request a protocol for this paper from *Bio-protocol*.

REFERENCES AND NOTES

1. T. J. Biden, E. Boslem, K. Y. Chu, N. Sue, Lipotoxic endoplasmic reticulum stress, β cell failure, and type 2 diabetes mellitus. *Trends Endocrinol. Metab.* **25**, 389–398 (2014).
2. R. H. Unger, M. G. Roth, A new biology of diabetes revealed by leptin. *Cell Metab.* **21**, 15–20 (2015).
3. J. C. Lo, S. Ljubicic, B. Leibiger, M. Kern, I. B. Leibiger, T. Moede, M. E. Kelly, D. C. Bhowmick, I. Murano, P. Cohen, A. S. Banks, M. J. Khandekar, A. Dietrich, J. S. Flier, S. Cinti, M. Blüher, N. N. Danial, P.-O. Berggren, B. M. Spiegelman, Adipsin is an adipokine that improves β cell function in diabetes. *Cell* **158**, 41–53 (2014).
4. Y.-S. Lee, C. Lee, J.-S. Choung, H.-S. Jung, H.-S. Jun, Glucagon-like peptide 1 increases β-cell regeneration by promoting α- to β-cell transdifferentiation. *Diabetes* **67**, 2601–2614 (2018).
5. A. Natalicchio, N. Marrano, G. Biondi, R. Spagnuolo, R. Labarbuta, I. Porreca, A. Cignarelli, M. Bugliani, P. Marchetti, S. Perrini, L. Laviola, F. Giorgino, The myokine irisin is released in response to saturated fatty acids and promotes pancreatic β-cell survival and insulin secretion. *Diabetes* **66**, 2849–2856 (2017).
6. J. Wei, T. Hanna, N. Suda, G. Karsenty, P. Ducy, Osteocalcin promotes β-cell proliferation during development and adulthood through Gprc6a. *Diabetes* **63**, 1021–1031 (2014).
7. T. J. Kieffer, R. S. Heller, J. F. Habener, Leptin receptors expressed on pancreatic β-cells. *Biochem. Biophys. Res. Commun.* **224**, 522–527 (1996).
8. J. Cantley, The control of insulin secretion by adipokines: Current evidence for adipocyte-beta cell endocrine signalling in metabolic homeostasis. *Mamm. Genome* **25**, 442–454 (2014).
9. P. Rorsman, F. M. Ashcroft, Pancreatic β-cell electrical activity and insulin secretion: Of mice and men. *Physiol. Rev.* **98**, 117–214 (2018).
10. M. A. Kalwat, M. H. Cobb, Mechanisms of the amplifying pathway of insulin secretion in the β cell. *Pharmacol. Ther.* **179**, 17–30 (2017).
11. E. Bourinet, M. E. Mangoni, J. Nargeot, Dissecting the functional role of different isoforms of the L-type Ca^{2+} channel. *J. Clin. Invest.* **113**, 1382–1384 (2004).
12. G. W. Zamponi, J. Striessnig, A. Koschak, A. C. Dolphin, The physiology, pathology, and pharmacology of voltage-gated calcium channels and their future therapeutic potential. *Pharmacol. Rev.* **67**, 821–870 (2015).
13. T. M. Reinbothe, S. Alkayyali, E. Ahlqvist, T. Tuomi, B. Isomaa, V. Lyssenko, E. Renström, The human L-type calcium channel Cav1.3 regulates insulin release and polymorphisms in CACNA1D associate with type 2 diabetes. *Diabetologia* **56**, 340–349 (2013).
14. G. Yang, Y. Shi, J. Yu, Y. Li, L. Yu, A. Welling, F. Hofmann, J. Striessnig, L. Juntti-Berggren, P.-O. Berggren, S.-N. Yang, CaV1.2 and CaV1.3 channel hyperactivation in mouse islet β cells exposed to type 1 diabetic serum. *Cell. Mol. Life Sci.* **72**, 1197–1207 (2015).
15. M. Braun, R. Ramracheya, M. Bengtsson, Q. Zhang, J. Karanauskaite, C. Partridge, P. R. Johnson, P. Rorsman, Voltage-gated ion channels in human pancreatic β-cells: Electrophysiological characterization and role in insulin secretion. *Diabetes* **57**, 1618–1628 (2008).
16. Y. Iwashima, W. Pugh, A. M. Depaoli, J. Takeda, S. Seino, G. I. Bell, K. S. Polonsky, Expression of calcium channel mRNAs in rat pancreatic islets and downregulation after glucose infusion. *Diabetes* **42**, 948–955 (1993).
17. T. L. Holtet, J. H. Graversen, I. Clemmensen, H. C. Thøgersen, M. Etzerodt, Tetranectin, a trimeric plasminogen-binding C-type lectin. *Protein Sci.* **6**, 1511–1515 (1997).
18. I. Clemmensen, L. C. Petersen, C. Kluft, Purification and characterization of a novel, oligomeric, plasminogen kringle 4 binding protein from human plasma: Tetranectin. *Eur. J. Biochem.* **156**, 327–333 (1986).
19. K. Ibaraki, C. A. Kozak, U. M. Wewer, R. Albrechtsen, M. F. Young, Mouse tetranectin: cDNA sequence, tissue-specific expression, and chromosomal mapping. *Mamm. Genome* **6**, 693–696 (1995).
20. L. Berglund, T. E. Petersen, The gene structure of tetranectin, a plasminogen binding protein. *FEBS Lett.* **309**, 15–19 (1992).
21. U. M. Wewer, K. Iba, M. E. Durkin, F. C. Nielsen, F. Loechel, B. J. Gilpin, W. Kuang, E. Engvall, R. Albrechtsen, Tetranectin is a novel marker for myogenesis during embryonic development, muscle regeneration, and muscle cell differentiation in vitro. *Dev. Biol.* **200**, 247–259 (1998).
22. U. M. Wewer, R. Albrechtsen, Tetranectin, a plasminogen kringle 4-binding protein. Cloning and gene expression pattern in human colon cancer. *Lab. Invest.* **67**, 253–262 (1992).
23. C. B. Sorensen, L. Berglund, T. E. Petersen, Cloning of a cDNA encoding murine tetranectin. *Gene* **152**, 243–245 (1995).
24. J. Kim, Y. S. Choi, S. Lim, K. Yea, J. H. Yoon, D.-J. Jun, S. H. Ha, J.-W. Kim, J. H. Kim, P.-G. Suh, S. H. Ryu, T. G. Lee, Comparative analysis of the secretory proteome of human adipose stromal vascular fraction cells during adipogenesis. *Proteomics* **10**, 394–405 (2010).
25. J.-T. Yang, Y.-J. Chen, C.-W. Huang, Y.-C. Wang, H. J. Mersmann, P.-H. Wang, S.-T. Ding, Docosahexaenoic acid suppresses expression of adipogenic tetranectin through sterol regulatory element-binding protein and forkhead box O protein in pigs. *Nutrients* **13**, 2315 (2021).
26. J. H. Graversen, R. H. Lorentsen, C. Jacobsen, S. K. Moestrup, B. W. Sigurskjold, H. C. Thogersen, M. Etzerodt, The plasminogen binding site of the C-type lectin tetranectin is located in the carbohydrate recognition domain, and binding is sensitive to both calcium and lysine. *J. Biol. Chem.* **273**, 29241–29246 (1998).
27. C. Kluft, A. F. Jie, P. Los, E. de Wit, L. Havekes, Functional analogy between lipoprotein(a) and plasminogen in the binding to the kringle 4 binding protein, tetranectin. *Biochem. Biophys. Res. Commun.* **161**, 427–433 (1989).
28. R. H. Lorentsen, J. H. Graversen, N. R. Caterer, H. C. Thogersen, M. Etzerodt, The heparin-binding site in tetranectin is located in the N-terminal region and binding does not involve the carbohydrate recognition domain. *Biochem. J.* **347**, 83–87 (2000).
29. U. M. Wewer, K. Ibaraki, P. Schjorring, M. E. Durkin, M. F. Young, R. Albrechtsen, A potential role for tetranectin in mineralization during osteogenesis. *J. Cell Biol.* **127**, 1767–1775 (1994).
30. E. S. Wang, X.-P. Zhang, H.-B. Yao, G. Wang, S.-W. Chen, W.-W. Gao, H.-J. Yao, Y.-R. Sun, C.-H. Xi, Y.-D. Ji, Tetranectin knockout mice develop features of Parkinson disease. *Cell. Physiol. Biochem.* **34**, 277–287 (2014).
31. G. Ferrannini, M. L. Manca, M. Magnoni, F. Andreotti, D. Andreini, R. Latini, A. Maseri, A. P. Maggioni, R. M. Ostroff, S. A. Williams, E. Ferrannini, Coronary artery disease and type 2 diabetes: A proteomic study. *Diabetes Care* **43**, 843–851 (2020).
32. Y. Chen, H. Han, X. Yan, F. Ding, X. Su, H. Wang, Q. Chen, L. Lu, R. Zhang, W. Jin, Tetranectin as a potential biomarker for stable coronary artery disease. *Sci. Rep.* **5**, 17632 (2015).
33. J. E. Ho, A. Lyass, P. Courchesne, G. Chen, C. Liu, X. Yin, S.-J. Hwang, J. M. Massaro, M. G. Larson, D. Levy, Protein biomarkers of cardiovascular disease and mortality in the community. *J. Am. Heart Assoc.* **7**, e008108 (2018).
34. C. Mylona-Karayanni, D. Gourgiotis, A. Bossios, E. F. Kamper, Oxidative stress and adhesion molecules in children with type 1 diabetes mellitus: A possible link. *Pediatr. Diabetes* **7**, 51–59 (2006).
35. L. Christensen, N. Johansen, B. A. Jensen, I. Clemmensen, Immunohistochemical localization of a novel, human plasma protein, tetranectin, in human endocrine tissues. *Histochemistry* **87**, 195–199 (1987).

36. M. Hermann, D. Pirkebner, A. Draxl, R. Margreiter, P. Hengster, In the search of potential human islet stem cells: Is tetranectin showing us the way? *Transplant. Proc.* **37**, 1322–1325 (2005).
37. Y. Ren, Y. Shi, Y. Wang, Y. Li, S. Wu, H. Li, Y. Zhang, H. Duan, p38 MAPK pathway is involved in high glucose-induced thioredoxin interacting protein induction in mouse mesangial cells. *FEBS Lett.* **584**, 3480–3485 (2010).
38. P. Patwari, L. J. Higgins, W. A. Chutkow, J. Yoshioka, R. T. Lee, The interaction of thioredoxin with Txnip. Evidence for formation of a mixed disulfide by disulfide exchange. *J. Biol. Chem.* **281**, 21884–21891 (2006).
39. F. Lin, P. Zhang, Z. Zuo, F. Wang, R. Bi, W. Shang, A. Wu, J. Ye, S. Li, X. Sun, J. Wu, L. Jiang, Thioredoxin-1 promotes colorectal cancer invasion and metastasis through crosstalk with S100P. *Cancer Lett.* **401**, 1–10 (2017).
40. Z. G. Hua, L. J. Xiong, C. Yan, D. H. Wei, Z. YingPai, Z. Y. Qing, Q. Z. Lin, F. R. Fei, W. Y. Ling, M. Z. Ren, Glucose and insulin stimulate lipogenesis in porcine adipocytes: Dissimilar and identical regulation pathway for key transcription factors. *Mol. Cells* **39**, 797–806 (2016).
41. Z. E. Floyd, J. M. Stephens, Controlling a master switch of adipocyte development and insulin sensitivity: Covalent modifications of PPARγ. *Biochim. Biophys. Acta* **1822**, 1090–1095 (2012).
42. S.-J. Han, Y. Zhang, I. Kim, K.-O. Chay, H. J. Yoon, D. I. Jang, S. Y. Yang, J. Park, H. A. Woo, I. Park, S.-R. Lee, Redox regulation of the tumor suppressor PTEN by the thioredoxin system and cumene hydroperoxide. *Free Radic. Biol. Med.* **112**, 277–286 (2017).
43. G. Powis, W. R. Montfort, Properties and biological activities of thioredoxins. *Annu. Rev. Biophys. Biomol. Struct.* **30**, 421–455 (2001).
44. Y. Guo, L. Einhorn, M. Kelley, K. Hirota, J. Yodoi, R. Reinbold, H. Scholer, H. Ramsey, R. Hromas, Redox regulation of the embryonic stem cell transcription factor oct-4 by thioredoxin. *Stem Cells* **22**, 259–264 (2004).
45. R. Retnakaran, C. K. Kramer, H. Choi, B. Swaminathan, B. Zinman, Liraglutide and the preservation of pancreatic β-cell function in early type 2 diabetes: The LIBRA trial. *Diabetes Care* **37**, 3270–3278 (2014).
46. Y. Fang, L. Ji, C. Zhu, Y. Xiao, J. Zhang, J. Lu, J. Yin, L. Wei, Liraglutide alleviates hepatic steatosis by activating the TFEB-regulated autophagy-lysosomal pathway. *Front. Cell Dev. Biol.* **8**, 602574 (2020).
47. Y. Jiang, Z. Wang, B. Ma, L. Fan, N. Yi, B. Lu, Q. Wang, R. Liu, GLP-1 improves adipocyte insulin sensitivity following induction of endoplasmic reticulum stress. *Front. Pharmacol.* **9**, 1168 (2018).
48. D. S. Hittel, W. E. Kraus, E. P. Hoffman, Skeletal muscle dictates the fibrinolytic state after exercise training in overweight men with characteristics of metabolic syndrome. *J. Physiol.* **548**, 401–410 (2003).
49. M. Saito, Y. Okamatsu-Ogura, M. Matsushita, K. Watanabe, T. Yoneshiro, J. Nio-Kobayashi, T. Iwanaga, M. Miyagawa, T. Kameya, K. Nakada, Y. Kawai, M. Tsujisaki, High incidence of metabolically active brown adipose tissue in healthy adult humans: Effects of cold exposure and adiposity. *Diabetes* **58**, 1526–1531 (2009).
50. B. Cannon, J. Nedergaard, Nonshivering thermogenesis and its adequate measurement in metabolic studies. *J. Exp. Biol.* **214**, 242–253 (2011).
51. K. Mukund, S. Subramaniam, Skeletal muscle: A review of molecular structure and function, in health and disease. *Wiley Interdiscip. Rev. Syst. Biol. Med.* **12**, e1462 (2020).
52. S. Hu, R. Kuwabara, B. J. de Haan, A. M. Smink, P. de Vos, Acetate and butyrate improve β-cell metabolism and mitochondrial respiration under oxidative stress. *Int. J. Mol. Sci.* **21**, 1542 (2020).
53. W. J. Schnedl, S. Ferber, J. H. Johnson, C. B. Newgard, STZ transport and cytotoxicity. Specific enhancement in GLUT2-expressing cells. *Diabetes* **43**, 1326–1333 (1994).
54. E. D. Buras, L. Yang, P. Saha, J. Kim, P. Mehta, Y. Yang, S. Hilsenbeck, H. Kojima, W. Chen, C. W. Smith, L. Chan, Proinsulin-producing, hyperglycemia-induced adipose tissue macrophages underlie insulin resistance in high fat-fed diabetic mice. *FASEB J.* **29**, 3537–3548 (2015).
55. S. E. Kahn, R. L. Hull, K. M. Utzschneider, Mechanisms linking obesity to insulin resistance and type 2 diabetes. *Nature* **444**, 840–846 (2006).
56. A. H. Xiang, E. Trigo, M. Martinez, N. Katkhouda, E. Beale, X. Wang, J. Wu, T. Chow, C. Montgomery, K. S. Nayak, F. Hendee, T. A. Buchanan; RISE Consortium; RISE Collaborators, Impact of gastric banding versus metformin on β-cell function in adults with impaired glucose tolerance or mild type 2 diabetes. *Diabetes Care* **41**, 2544–2551 (2018).
57. Y. Lin, A. H. Berg, P. Iyengar, T. K. T. Lam, A. Giacca, T. P. Combs, M. W. Rajala, X. Du, B. Rollman, W. Li, M. Hawkins, N. Barzilai, C. J. Rhodes, I. G. Fantus, M. Brownlee, P. E. Scherer, The hyperglycemia-induced inflammatory response in adipocytes: The role of reactive oxygen species. *J. Biol. Chem.* **280**, 4617–4626 (2005).
58. T. Mahdi, S. Hänzelmann, A. Salehi, S. J. Muhammed, T. M. Reinbothe, Y. Tang, A. S. Axelsson, Y. Zhou, X. Jing, P. Almgren, U. Krus, J. Taneera, A. M. Blom, V. Lyssenko, J. L. S. Esguerra, O. Hansson, L. Eliasson, J. Derry, E. Zhang, C. B. Wollheim, L. Groop, E. Renström, A. H. Rosengren, Secreted frizzled-related protein 4 reduces insulin secretion and is overexpressed in type 2 diabetes. *Cell Metab.* **16**, 625–633 (2012).
59. R. Huang, S. Yin, Y. Ye, N. Chen, S. Luo, M. Xia, L. Zhao, Circulating retinol-binding protein 4 is inversely associated with pancreatic β-cell function across the spectrum of glycemia. *Diabetes Care* **43**, 1258–1265 (2020).
60. E. F. Kamper, L. Kopeikina, A. Mantas, C. Stefanadis, P. Toutouzas, J. Stavridis, Tetranectin levels in patients with acute myocardial infarction and their alterations during thrombolytic treatment. *Ann. Clin. Biochem.* **35**, 400–407 (1998).
61. K. McDonald, N. Glezeva, P. Collier, J. O'Reilly, E. O'Connell, I. Tea, A. Russell-Hallinan, C. Tonry, S. Pennington, J. Gallagher, M. Ledwidge, J. Baugh, C. J. Watson, Tetranectin, a potential novel diagnostic biomarker of heart failure, is expressed within the myocardium and associates with cardiac fibrosis. *Sci. Rep.* **10**, 7507 (2020).
62. A. Pingitore, I. Ruz-Maldonado, B. Liu, G. C. Huang, P. Choudhary, S. J. Persaud, Dynamic profiling of insulin secretion and ATP generation in isolated human and mouse islets reveals differential glucose sensitivity. *Cell. Physiol. Biochem.* **44**, 1352–1359 (2017).
63. O. Cabrera, D. M. Berman, N. S. Kenyon, C. Ricordi, P. O. Berggren, A. Caicedo, The unique cytoarchitecture of human pancreatic islets has implications for islet cell function. *Proc. Natl. Acad. Sci. U.S.A.* **103**, 2334–2339 (2006).
64. Y. Kang, X. Huang, E. A. Pasyk, J. Ji, G. G. Holz, M. B. Wheeler, R. G. Tsushima, H. Y. Gaisano, Syntaxin-3 and syntaxin-1A inhibit L-type calcium channel activity, insulin biosynthesis and exocytosis in beta-cell lines. *Diabetologia* **45**, 231–241 (2002).
65. T. Mogues, M. Etzerodt, C. Hall, G. Engelich, J. H. Graversen, K. L. Hartshorn, Tetranectin binds to the kringle 1-4 form of angiostatin and modifies its functional activity. *J. Biomed. Biotechnol.* **2004**, 73–78 (2004).
66. S. Nielbo, J. K. Thomsen, J. H. Graversen, P. H. Jensen, M. Etzerodt, F. M. Poulsen, H. C. Thøgersen, Structure of the plasminogen kringle 4 binding calcium-free form of the C-type lectin-like domain of tetranectin. *Biochemistry* **43**, 8636–8643 (2004).
67. K. G. Alberti, P. Zimmet, J. Shaw; IDF Epidemiology Task Force Consensus Group, The metabolic syndrome—A new worldwide definition. *Lancet* **366**, 1059–1562 (2005).
68. American Diabetes Association, 2. Classification and diagnosis of diabetes: Standards of medical care in diabetes—2020. *Diabetes Care* **43**, S14–S31 (2020).
69. C. J. Fan, K. Hirose, C. M. Walsh, M. Quartuccio, N. M. Desai, V. K. Singh, R. R. Kalyani, D. S. Warren, Z. Sun, M. N. Hanna, M. A. Makary, Laparoscopic total pancreatectomy with islet autotransplantation and intraoperative islet separation as a treatment for patients with chronic pancreatitis. *JAMA Surg.* **152**, 550–556 (2017).
70. H. Zhou, J. Dai, Q. H. Sheng, R. X. Li, C. H. Shieh, A. Guttman, R. Zeng, A fully automated 2-D LC-MS method utilizing online continuous pH and RP gradients for global proteome analysis. *Electrophoresis* **28**, 4311–4319 (2007).
71. L. Sauma, N. Franck, J. F. Paulsson, G. T. Westermark, P. Kjolhede, P. Stralfors, M. Söderström, F. H. Nystrom, Peroxisome proliferator activated receptor gamma activity is low in mature primary human visceral adipocytes. *Diabetologia* **50**, 195–201 (2007).
72. G. X. Wang, X.-Y. Zhao, Z.-X. Meng, M. Kern, A. Dietrich, Z. Chen, Z. Cozacov, D. Zhou, A. L. Okunade, X. Su, S. Li, M. Blüher, J. D. Lin, The brown fat-enriched secreted factor Nrg4 preserves metabolic homeostasis through attenuation of hepatic lipogenesis. *Nat. Med.* **20**, 1436–1443 (2014).
73. J. Zhang, N. Zhang, M. Liu, X. Li, L. Zhou, W. Huang, Z. Xu, J. Liu, N. Musi, R. A. DeFronzo, J. M. Cunningham, Z. Zhou, X.-Y. Lu, F. Liu, Disruption of growth factor receptor-binding protein 10 in the pancreas enhances β-cell proliferation and protects mice from streptozotocin-induced β-cell apoptosis. *Diabetes* **61**, 3189–3198 (2012).
74. M. R. Marasco, A. M. Conteh, C. A. Reissaus, J. E. Cupit V, E. M. Appleman, R. G. Mirmira, A. K. Linnemann, Interleukin-6 reduces β-cell oxidative stress by linking autophagy with the antioxidant response. *Diabetes* **67**, 1576–1588 (2018).
75. G. Tang, Y. Wang, S. Park, N. S. Bajpayee, D. Vi, Y. Nagaoka, L. Birnbaumer, M. Jiang, Go2 G protein mediates galanin inhibitory effects on insulin release from pancreatic β cells. *Proc. Natl. Acad. Sci. U.S.A.* **109**, 2636–2641 (2012).
76. X. L. Lou, X. Yu, X.-K. Chen, K.-L. Duan, L.-M. He, A.-L. Qu, T. Xu, Z. Zhou, Na^+ channel inactivation: A comparative study between pancreatic islet beta-cells and adrenal chromaffin cells in rat. *J. Physiol.* **548**, 191–202 (2003).
77. Y. Perez-Riverol, A. Csordas, J. Bai, M. Bernal-Llinares, S. Hewapathirana, D. J. Kundu, A. Inuganti, J. Griss, G. Mayer, M. Eisenacher, E. Pérez, J. Uszkoreit, J. Pfeuffer, T. Sachsenberg, Ş. Yılmaz, S. Tiwary, J. Cox, E. Audain, M. Walzer, A. F. Jarnuczak, T. Ternent, A. Brazma, J. A. Vizcaíno, The PRIDE database and related tools and resources in 2019: Improving support for quantification data. *Nucleic Acids Res.* **47**, D442–D450 (2019).
78. M. Liu, L. Zhou, A. Xu, K. S. L. Lam, M. D. Wetzel, R. Xiang, J. Zhang, X. Xin, L. Q. Dong, F. Liu, A disulfide-bond A oxidoreductase-like protein (DsbA-L) regulates adiponectin multimerization. *Proc. Natl. Acad. Sci. U.S.A.* **105**, 18302–18307 (2008).

Acknowledgments: We thank the OE Biotech Co. Ltd. (Shanghai) for the RNA sequencing.
Funding: This work was supported by grants from the National Key Research and Development Program (2019YFA0801900 and 2018YFC2000100), the National Natural Science Foundation of China (91749118, 81730022, and 81770775), and the Planned Science and Technology

Project of Hunan Province (2017RS3015). **Author contributions:** Conceptualization: J.Z. and Feng Liu. Supervision: J.Z., Feng Liu, C.T., J.B., and Z.Z. Investigation: Fen Liu, Z.C., Y.Y., G.P., P.Z., X.W., D.L., H.L., L.F., Z.X., Y.J., R.Z., and R.L. Visualization: Fen Liu and Z.C. Resources: E.W., T.L., S.H., L.S., S.Y., and R.X. Writing—original draft: J.Z., Fen Liu, and Z.C. Reviewing, editing, and funding acquisition: J.Z. and Feng Liu. **Competing interests:** The authors declare that they have no competing interests. **Data and materials availability:** All data needed to evaluate the conclusions in the paper are present in the paper and/or the Supplementary Materials. Moreover, the mass spectrometry proteomics data have been deposited to the ProteomeXchange Consortium (http://proteomecentral.proteomexchange.org) via the iProX partner repository with the dataset identifier PXD035512 (*77*). The RNA sequencing data have been deposited as a BioProject under accession PRJNA859403.

Submitted 23 March 2022
Accepted 4 August 2022
Published 21 September 2022
10.1126/sciadv.abq1799